https://doi.org/10.5194/egusphere-2025-6014
Preprint. Discussion started: 6 January 2026

Scale-Dependent Transition in Soil Moisture Memory and Its Environmental Controls in Complex Mountain Terrain

Jun Zhang[1,2,3], Songtang He[1*], Yong Li[1], Yuan Xue[2]

[1] Key Laboratory of Mountain Hazards and Engineering Resilience /Institute of Mountain Hazards and Environment, Chinese Academy of Sciences, Chengdu 610041, China

[2] State Key Laboratory of Hydroscience and Engineering; Department of Hydraulic Engineering, Tsinghua University, Beijing 100084, China

[3] University of Chinese Academy of Sciences, Beijing 100049, China

Correspondence: Songtang He (hest@imde.ac.cn)

Abstract: Soil moisture memory (SMM) defines the antecedent wetness states that modulate catchment responses to meteorological triggers, serving as a critical determinant of background hydraulic susceptibility. However, its multi-scale characteristics and environmental drivers remain poorly understood in complex terrain. This study characterizes SMM dynamics across daily-to-interannual scales using daily data (2003 – 2022) from three hazard-prone watersheds in southwestern China (Dali River, Anning River, and Jiangjia Ravine). By integrating Power Spectrum Analysis, Detrended Fluctuation Analysis (DFA-2), and a spatial attribution modeling framework, we identify a distinct scale-dependent transition in SMM persistence and its controls. Results revealed that while memory intensity generally weakened with scale, humid catchments exhibited a robust "inherent persistence" regime extending to multi-year scales. Crucially, feature importance analysis uncovered a structural transition at approximately the 5-year scale: atmospheric variables and vegetation dominated short-term variability, whereas soil properties and topography governed the system's long-term capacity to integrate low-frequency signals. Mechanistically, this marks a shift from event-driven hydraulic responses to background storage trends regulated by deep

https://doi.org/10.5194/egusphere-2025-6014
Preprint. Discussion started: 6 January 2026

soil buffering. These findings provide a basis for distinguishing event-scale hydraulic preconditioning from long-term background susceptibility, offering a conceptual framework for incorporating operational persistence horizons into hierarchical hazard assessment strategies.

Keywords: Soil moisture memory; Driving Factor; Persistence horizon; Power spectrum analysis; Detrended fluctuation analysis

1. Introduction

Soil moisture memory (SMM) is a critical driver of mountain hazards, including debris flows, landslides, and soil erosion (An et al., 2025; Hu et al., 2015; Moragoda et al., 2022). Mechanistically, elevated soil moisture reduces effective stress and shear strength by increasing pore water pressure, thereby predisposing slopes to instability. While precipitation acts as the immediate trigger, antecedent soil moisture conditions the landscape's susceptibility by determining how close the system is to its critical failure thresholds (Bogaard et al., 2018; Cai et al., 2019). Beyond this immediate mechanical role, the persistence of SMM, quantified by its memory length, theoretically defines the timescale over which antecedent signals persist, providing essential information on hydraulic preconditioning for early warning systems (Huang et al., 2022; Wicki et al., 2020). However, translating this theoretical memory into operational forecasts requires further validation against historical hazard events.

Empirical evidence from various hazards supports this mechanistic understanding. Specifically, landslide probability increases exponentially when soil moisture (a proxy for pore-water pressure saturation) exceeds a critical threshold of 30 ~ 40 % (Mirus et al., 2018; Wicki et al., 2021). While

https://doi.org/10.5194/egusphere-2025-6014
Preprint. Discussion started: 6 January 2026

these studies define the critical state, quantifying the SMM persistence provides the essential temporal window required to estimate how long antecedent rainfall continues to drive the system toward this saturation threshold (Mirus et al., 2018). For debris flows, antecedent soil moisture conditions determine not only the likelihood of initiation but also the potential runout distance (Coe et al., 2008). Furthermore, under identical rainfall intensity, the soil loss rate can be 3 to 5 times higher under wet antecedent conditions than under dry conditions (Ran et al., 2012). Collectively, this evidence highlights the fundamental importance of quantifying SMM to understand how antecedent conditions modulate hazard initiation thresholds. Nonetheless, a comprehensive, multi-scale characterization of how SMM evolves from monthly to seasonal, annual, and multi-year scales remains limited (Entin et al., 2000; Nicolai-Shaw et al., 2016; Zhang et al., 2025). Unlike immediate meteorological triggers, this multi-scale memory reflects the system's inertia and defines the baseline hydrological state of the catchment in response to external forcing. However, elucidating its drivers is challenging due to the combined effects of diverse factors—topographic, pedological, meteorological, and vegetation (Brocca et al., 2007; Dong et al., 2018; Schönauer et al., 2024; Varga et al., 2020). Their strong interactions further complicate the disentanglement of individual and joint effects (Peng et al., 2023).

Previous studies have explored driving factors of soil moisture variability at discrete temporal scales (Blanka-Végi et al., 2025; Cho et al., 2014; Fang et al., 2016; Kursa et al., 2010), identifying, for instance, wilting point and evapotranspiration as key at the annual scale (Blanka-Végi et al., 2025) or vegetation type at the monthly scale (Fang et al., 2016). However, by focusing on individual scales, these studies have seldom established a systematic hierarchy of the relative importance between static and dynamic factors across continuous temporal scales. This lack of a

https://doi.org/10.5194/egusphere-2025-6014
Preprint. Discussion started: 6 January 2026

unified, scale-explicit framework prevents a mechanistic understanding of SMM persistence and limits the development of hazard assessment models capable of distinguishing background hydraulic loading from immediate event triggering (Li et al., 2025; Zhang et al., 2024).

While previous studies have established the existence of soil moisture memory (SMM) and its general scale dependence at global or continental scales (e.g., Entin et al., 2000; Nicolai-Shaw et al., 2016), a critical gap persists in mechanistically linking this multi-scale memory to specific hydrological processes and practical hazard prediction within the complex terrain where these hazards predominantly occur. To bridge this gap, this study leverages a two-decade-long daily soil moisture dataset across three contrasting, hazard-prone watersheds with the following objectives: (1) to quantify the scale-transition threshold and hierarchical drivers of SMM; (2) to establish a quantitative hierarchy of driving factors across temporal scales; and (3) to develop a conceptual framework linking multi-scale SMM to differentiated hazard preconditioning mechanisms. While direct validation against site-specific hazard inventories is beyond our current scope due to the spatial resolution mismatch (1-km pixels vs. slope-scale failures), we synthesize our findings with published hazard-SMM relationships (e.g., Mirus et al., 2018; Wei et al., 2025) to demonstrate the potential for SMM-informed early warning systems. The paper is structured as follows: Section 2 describes the study areas, data, and methods. Section 3 presents the results, which are discussed in Section 4. Finally, Section 5 provides the main conclusions.

2. Materials and Methods

This study investigates soil moisture (SM) dynamics and their drivers across three hydro-climatically and geomorphologically distinct watersheds: the Dali River Basin, Anning River Basin, and Jiangjia Ravine. We incorporated static and dynamic variables—spanning topography, soil

https://doi.org/10.5194/egusphere-2025-6014
Preprint. Discussion started: 6 January 2026

properties, meteorological conditions, and vegetation indices—from multiple authoritative datasets. SM temporal memory and persistence horizons were quantified using Power Spectral Analysis (PSA) and second-order Detrended Fluctuation Analysis (DFA-2), respectively, while the Boruta–Random Forest algorithm was employed to quantify variable importance across spatial and temporal scales. The overall research framework is illustrated in Fig. 1.

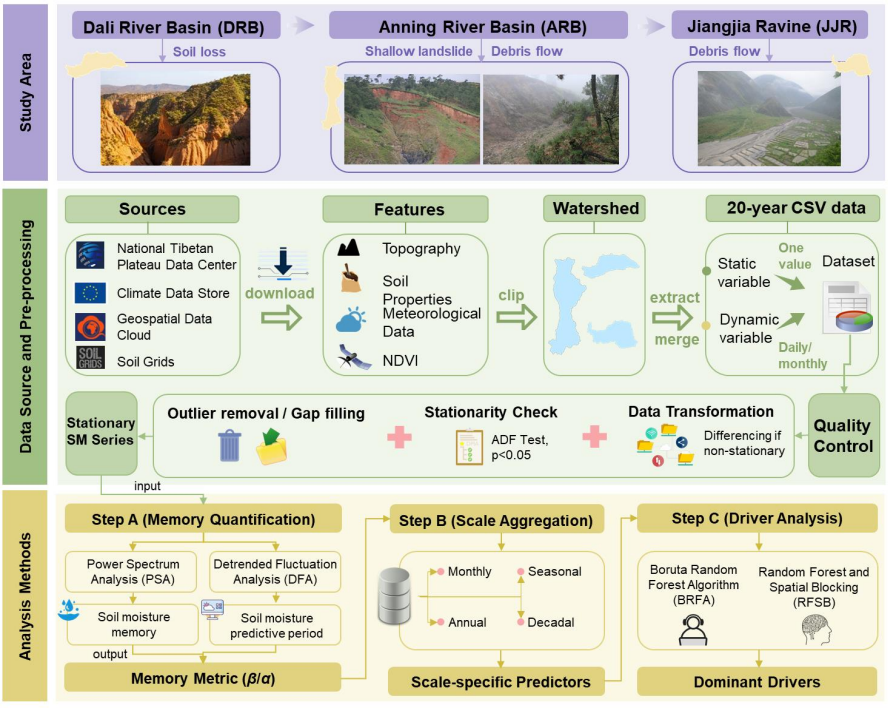

Fig. 1 Research framework of this study. The workflow integrates multi-source data processing, memory quantification, and driver identification. Key pre-processing steps include outlier removal and stationarity checks (ADF test) to ensure time stability. Soil moisture memory is quantified using Power Spectrum Analysis (PSA) and Detrended Fluctuation Analysis (DFA-2), followed by a multi-scale driver analysis using the Boruta algorithm across monthly to decadal aggregation windows.

https://doi.org/10.5194/egusphere-2025-6014
Preprint. Discussion started: 6 January 2026

2.1 Study Area

We selected three hydro-climatically distinct watersheds in southwestern China to represent a spectrum of mountain hazard environments (Fig. 2; detailed physiographic characteristics are provided in Appendix B and Table B1).

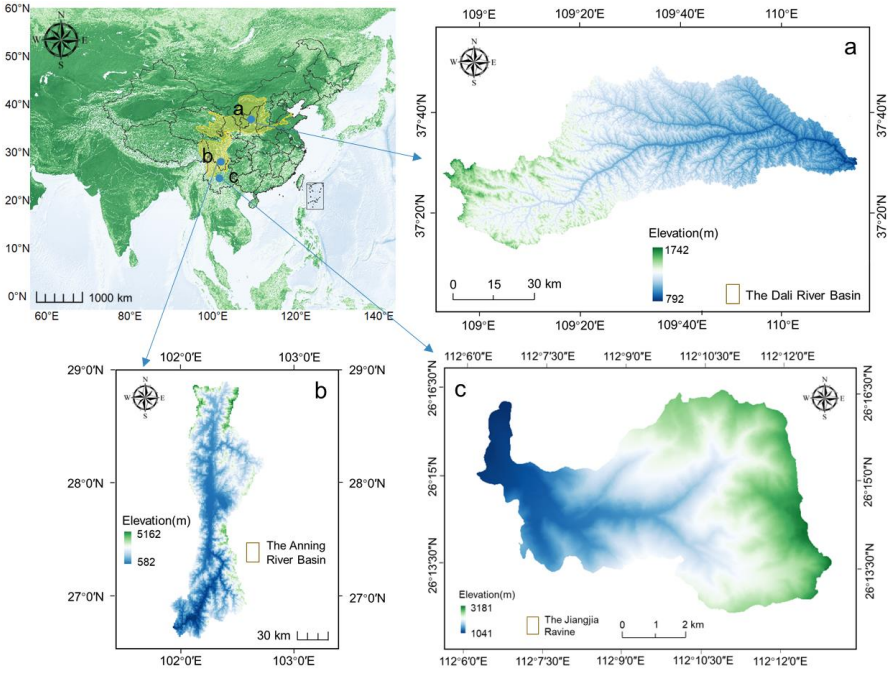

Fig. 2 Location of the study areas: (a) the Dali River Basin (DRB), (b) the Anning River Basin, (c) the Jiangjia Ravine.

- **Dali River Basin (DRB):** Semi-Arid Erosion-Prone System. Located on the Chinese Loess Plateau (3,906 km^2), the DRB features steep loess terrain (avg. slope 17°) and highly erodible soils (silt > 60 %). The climate is semi-arid continental, with precipitation highly concentrated in summer storms (> 70 % from May to September), leading to persistent soil moisture deficits and severe erosion rates (Liu et al., 2020; Zhang et al.,

https://doi.org/10.5194/egusphere-2025-6014
Preprint. Discussion started: 6 January 2026

2023).

- **Anning River Basin (ARB):** Complex Mountain-Valley System. Situated in southwestern Sichuan (11,150 km^2), the ARB is characterized by dramatic relief (900–4,750 m) and vertical climatic zonation. It operates under a humid subtropical-monsoon climate (~ 1,070 mm rainfall) with dense forest cover (Chen et al., 2024). Consequently, soil moisture dynamics are strongly regulated by vegetation phenology and the buffering capacity of deep forest soils (Yin et al., 2020).
- **Jiangjia Ravine (JJR):** Debris-Flow Dominated Catchment. A small (48.6 km^2) but extremely steep catchment in the Xiaojiang fault zone. Intense monsoon rainfall (> 85 % in May–Oct) combined with fractured geology drives rapid hydrological response cycles: rapid saturation during storms followed by quick drainage (Yang et al., 2023). This makes JJR a classic environment for high-frequency debris flows (Wei et al., 2025).

2.2 Data Sources and Preprocessing

We constructed a dataset comprising 12 static and dynamic covariates (Table 1) alongside daily soil moisture (SM) data (1-km resolution) for the period 2003–2022.

Soil Moisture Dataset: We utilized the all-weather 1-km daily soil moisture (SM) product developed by Song et al. (2022) for the period 2003–2022. Unlike raw reanalysis data or coarse passive microwave retrievals, this dataset employs a machine learning-based spatiotemporal reconstruction framework to generate seamless high-resolution estimates. Specifically, it downscales and fuses coarse-resolution passive microwave observations (AMSR-E/2) with high-resolution optical/thermal land surface parameters (MODIS) and meteorological forcing (ERA5-Land), using a random forest algorithm trained on extensive ground observations.

https://doi.org/10.5194/egusphere-2025-6014
Preprint. Discussion started: 6 January 2026

Validation and Uncertainty: This product was selected for its capacity to resolve hillslope-scale heterogeneity in complex terrain, a critical requirement for our hazard-focused analysis. Comprehensive validation against approximately 2,400 in-situ stations across China demonstrates robust accuracy, with an average correlation coefficient (R) of 0.89 and an unbiased Root Mean Square Error (ubRMSE) of 0.053 m^3/m^3 (Song et al., 2022). While we acknowledge the inherent uncertainties associated with microwave retrieval in mountainous regions (e.g., geometric distortion and shadowing effects), this dataset represents the state-of-the-art balance between spatial resolution and temporal continuity. Furthermore, since our study focuses on the temporal persistence features (spectral exponents) rather than absolute magnitudes, the potential systematic bias in complex terrain has minimal impact on the derived memory metrics (see Appendix C for further discussion on data reliability and preprocessing).

Table 1. Static and dynamic covariates used in the final modeling framework and the target variable (soil moisture, SM).

Types	Variable (abbreviation)	Description	Units	Source
Static	Slope (β)	Rate of change of elevation at each pixel (DEM-derived)	°	Geospatial Data Cloud (DEM)
	Aspect (Asp)	Orientation of the steepest downslope (DEM-derived)	°	
	Topographic Wetness Index (TWI)	Potential wetness index based on slope and upslope contributing area (DEM-derived)	-	
	Soil texture (Sand, Silt, Clay)	Mass fractions of soil particle-size classes	g/kg	Soil Grids
	Normalized Difference Vegetation Index (NDVI)	Vegetation greenness from red and NIR reflectance	-	Gao et al., 2022
Dynamic	Precipitation (Prec.)	Daily total precipitation	mm	Xie et al., 2019
	Surface wind speed (WS)	Mean daily wind speed at 10 m height	m/s	ERA5 (Hersbach

https://doi.org/10.5194/egusphere-2025-6014
Preprint. Discussion started: 6 January 2026

	Relative humidity (rhu)	Ratio of actual to saturated vapor pressure	%	et al., 2023)
	2m air temperature (T_{2m})	Daily mean air temperature at 2 m height	°C	
	Actual evaporation (AE)	Daily actual evapotranspiration	mm/day	
Target	Soil moisture (SM)	Volumetric soil water content	cm^3/cm^3	Song et al., 2022

Auxiliary static variables (e.g., soil texture, TWI) represent basin physiography, while dynamic variables (e.g., precipitation, NDVI) capture climate-vegetation interactions. All data were resampled to a uniform 1-km grid. Preprocessing included linear interpolation for short gaps (≤ 3 days), outlier removal, and stationarity checks using the Augmented Dickey-Fuller test (details in Appendix C).

2.3 Quantifying Soil Moisture Memory (PSA and DFA-2)

To characterize the multi-scale persistence of soil moisture, we employed two complementary spectral techniques. Crucially, given the 20-year length of our dataset (2003 – 2022), distinct statistical limitations exist for resolving low-frequency dynamics. Following the standard signal processing constraint which requires the time series length (N) to be significantly longer than the timescale of interest (T) for robust estimation (typically $N \geq 3T$), we explicitly distinguish between two regimes:

1. **Reliable Memory Window ($T \leq 7$ years):** Timescales where sufficient realizations (approx. N/3) exist to statistically verify dynamic persistence and oscillatory behavior.
2. **Low-Frequency Background State ($T > 7$ years):** The lowest frequency components, which are interpreted as basin storage trends or decadal climatic regime shifts, rather than verifiable memory cycles.

https://doi.org/10.5194/egusphere-2025-6014
Preprint. Discussion started: 6 January 2026

First, Power Spectrum Analysis (PSA) was utilized to diagnose the strength of temporal memory in the frequency domain. By estimating the spectral exponent (β), PSA effectively distinguishes memory-driven processes (red noise, $\beta > 0$) from random meteorological inputs (white noise, $\beta \approx 0$). In this study, β values derived within the Reliable Memory Window (seasonal to ~7 years) are used to quantify interannual persistence, whereas values in the Low-Frequency Background (> 7 years) serve only as indicators of the quasi-static mean-state stability.

Second, to account for the non-stationarity inherent in long-term hydrological records, we applied the second-order Detrended Fluctuation Analysis (DFA-2). Unlike standard autocorrelation, DFA-2 filters out polynomial trends to reveal intrinsic correlation structures. Cross-validation with the standard Autocorrelation Function (ACF) further confirms the robustness of these DFA-2 metrics (see Fig. E1 in Appendix). We specifically identified "persistence horizons"—time windows where the fluctuation exponent (α) exceeds 0.9. Consistent with the PSA framework defined above, persistence horizons extending beyond the 7-year threshold are classified as "Background Preconditioning" baselines, distinct from the active dynamic memory observed at shorter scales. Detailed mathematical formulations, including the phase-randomization significance testing, are provided in Appendix A.

2.4 Identifying Predictors via a Spatial Attribution Modeling Framework

To determine the hierarchical importance of environmental predictors, we utilized the Boruta feature selection algorithm wrapped around a Random Forest regressor. Given that SMM is a temporal statistic derived from time series, while landscape attributes are spatially heterogeneous, we constructed a spatial attribution framework to link these dimensions.

In this approach, the temporal memory metric calculated for each pixel (e.g., the spectral

https://doi.org/10.5194/egusphere-2025-6014
Preprint. Discussion started: 6 January 2026

exponent β) serves as the spatial response variable. This target was regressed against a suite of spatially distributed predictors, which were categorized into two groups:

1. **Static variables:** Landscape properties that remain constant over the study period (e.g., soil texture, slope, TWI).
2. **Aggregated dynamic variables:** Time-varying meteorological and vegetation data aggregated to match the temporal scale of the memory metric (e.g., mean decadal NDVI or total precipitation).

This construction allows us to quantify how spatial heterogeneity in static and dynamic boundary conditions correlates with the temporal persistence of soil moisture. Feature importance was validated using spatial block cross-validation to account for spatial autocorrelation (details in Appendix D).

It is essential to emphasize that the "Space-for-Time" framework employed here identifies statistical associations rather than establishing causal relationships. The Boruta-RF algorithm ranks predictors by their capacity to explain spatial variance in temporal memory metrics, but fundamentally cannot distinguish between: (i) direct causal drivers, (ii) proxy variables correlated with unmeasured causal factors, or (iii) response variables involved in bidirectional feedback loops.

Furthermore, the physical collinearity inherent in mountain landscapes—often termed the "catena concept"—means that soil texture and topography co-evolve along hillslopes: steep upper slopes typically develop shallow, coarse-textured soils with rapid drainage, whereas convergent lower slopes accumulate deep, clay-rich deposits with enhanced water retention. Consequently, high importance scores for both Slope and Clay content (Section 3.3) likely reflect this coupled landscape structure rather than fully independent effects.

https://doi.org/10.5194/egusphere-2025-6014
Preprint. Discussion started: 6 January 2026

To partially address these limitations, we: (1) interpret the identified associations through the lens of established hydrological theory (e.g., linear reservoir models; Section 4.1), providing mechanistic plausibility for the observed statistical patterns; and (2) conduct partial correlation analysis controlling for topographic variables (Appendix G) to assess the robustness of soil-SMM associations against landscape confounding. However, readers should note that our framework is designed to generate testable hypotheses about SMM predictors rather than to confirm causal mechanisms, which would require controlled experiments or instrumental variable approaches beyond the scope of remote sensing analysis.

3. Results

3.1 Power Spectrum Analysis of SM Memory

It is important to note that while spectral analyses are presented up to the 20-year scale to illustrate trends, quantitative interpretations are explicitly distinguished based on the record length constraint. We define the 1–7 year range as the "Reliable Spectral Window" for dynamic memory estimation ($N \geq 3T$). Results beyond this threshold (> 7 years) are interpreted as the "Low-Frequency Background State," reflecting the system's convergence to equilibrium rather than oscillatory persistence.

Power spectrum analysis revealed the scale-dependent characteristics of soil moisture memory (SMM) across the three basins (Fig. 3). All reported spectral exponents (β) are presented as the mean estimate ± the 95 % confidence interval derived from the log–log regression. Extensive sensitivity tests (detailed in Appendix E, Table E4 and Fig. E2) further confirm that these spectral patterns are robust to variations in detrending orders and frequency cutoffs, with the spatial ranking of memory strength remaining highly consistent (Spearman's $\rho > 0.92$) across parameter sets.

https://doi.org/10.5194/egusphere-2025-6014
Preprint. Discussion started: 6 January 2026

At short timescales (within one year), memory during individual rainy season months was consistently weaker than that of the integrated rainy season period, whereas dry season months showed stronger memory than the overall dry season aggregate (Fig. 3a–1, b–1, c–1).

Over longer intervals (1-20 years), SMM declined progressively. Within the reliable window, the hierarchical trend generally follows $\beta_{1\text{-yr}} > \beta_{5\text{-yr}}$. Beyond this point, in the low-frequency background zone (> 7 years), the metrics stabilized, capturing the basin's static storage baseline (Fig. 3a–2, b–2, c–2).

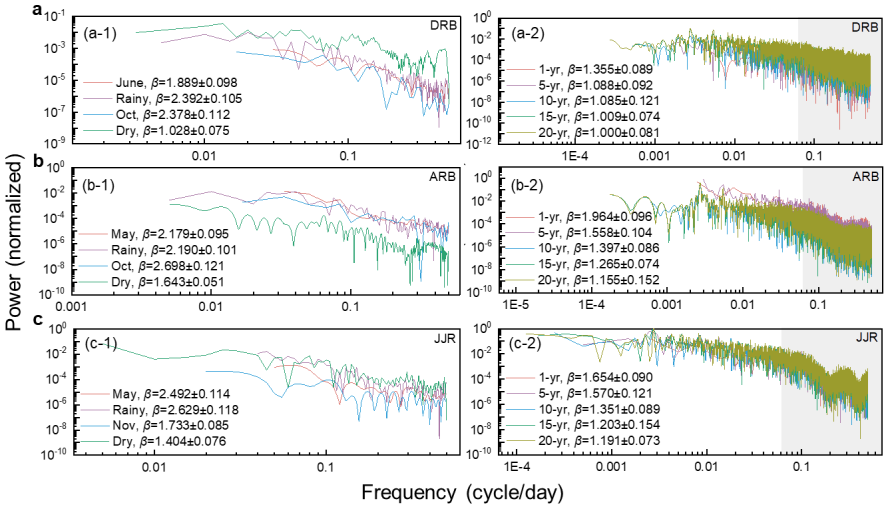

Fig. 3 Power spectrum analysis of soil moisture memory in the (a) Dali River Basin (DRB), (b) Anning River Basin (ARB), and (c) Jiangjia Ravine (JJR). Left panels show normalized power spectra at intra-annual scales (months and aggregated seasons). Right panels show inter-annual spectra (1 ~ 20 years). The spectral exponent (β, mean ± 95% CI) quantifies memory strength, with higher values indicating stronger long-term persistence. The gray shaded region (Time Scale > 1825 days) denotes where spectral estimation is limited by the 20-year data record; results here should be interpreted as low-frequency trends rather than robust spectral features. CI, confidence interval.

In the Dali River Basin (DRB), the full rainy season memory (β = 2.392 ± 0.105), calculated

https://doi.org/10.5194/egusphere-2025-6014
Preprint. Discussion started: 6 January 2026

over the continuous period from June to September, was significantly stronger than that of the initial month (June, $\beta = 1.889 \pm 0.098$). In contrast, the integrated dry season memory ($\beta = 1.028 \pm 0.075$) was considerably weaker than that of October ($\beta = 2.378 \pm 0.112$) (Fig. 3a-1). At interannual scales, SMM systematically declines from $\beta = 1.355 \pm 0.089$ (1-year) to $\beta = 1.000 \pm 0.081$ (20-year) (background state) (Fig. 3a-2).

In the Anning River Basin (ARB), the integrated rainy season memory ($\beta = 2.190 \pm 0.101$) is slightly stronger than that of May ($\beta = 2.179 \pm 0.095$), peaking in October ($\beta = 2.698 \pm 0.121$) (Fig. 3b-1). At interannual scales, the ARB had the highest SMM among the basins, with a mean β of 1.468 ± 0.084 — exceeding the DRB (1.107 ± 0.072) and JJR (1.394 ± 0.079) — and decreased gradually from 1.964 ± 0.096 (1-year) to 1.265 ± 0.074 (20-year) (background state) (Fig. 3b-2).

In the Jiangjia Ravine (JJR), SMM peaks during the rainy season (May: $\beta = 2.492 \pm 0.114$; full rainy season: $\beta = 2.629 \pm 0.118$), whereas it weakened during the dry season (Nov: $\beta = 1.733 \pm 0.085$; full dry season: $\beta = 1.404 \pm 0.076$) (Fig. 3c-1). At interannual scales, the JJR exhibited an intermediate level of SMM — stronger than that of the DRB but weaker than the ARB — with β values decreasing from 1.654 ± 0.090 (1-year) to 1.191 ± 0.073 (20-year) (background state) (Fig. 3c-2).

3.2 DFA-2 Analysis of SM Persistence Horizons

Based on the memory characteristics identified by PSA, we next quantified the associated persistence horizons using DFA-2. All reported α values in the high-memory range ($\alpha \geq 0.9$) were statistically significant ($p < 0.01$) based on phase-randomization surrogate testing (see Appendix A). Soil moisture persistence exhibited distinct spatiotemporal patterns across the three basins (Fig. 4). In the Dali River Basin (DRB), persistence was short during the early rainy season (24-30 days in

https://doi.org/10.5194/egusphere-2025-6014
Preprint. Discussion started: 6 January 2026

June) but extends substantially through the full rainy season (41-122 days); in contrast, October showed almost no persistence (Fig. 4a-1). During the dry season, persistence increased to 61-95 days, indicating a stronger influence of soil properties under limited rainfall. Beyond the seasonal scale, the characteristic persistence horizon increased moderately from 31-73 days (1-year) to 174-429 days (20-year), peaking between 10 and 15 years (Fig. 4a-2).

The Anning River Basin (ARB) exhibited the longest persistence horizons across all temporal scales, with all reported ranges being statistically significant ($p < 0.05$) based on the DFA-2 significance testing procedure described in Section 2.4 (2). At the monthly scale, persistence ranged from 17-31 days in May to 25–31 days in October, and these durations increased markedly at the seasonal scale—reaching 37-184 days during the rainy season and 47-76 days during the dry season (Fig. 4b-1). Beyond the seasonal scale, the persistence horizon rose sharply from 40-71 days (1-year) to 236-728 days (20-year) (Fig. 4b-2). This extended memory window, particularly at the multi-year scale, implies that the basin's soil moisture state tracks the low-frequency signals of inter-annual climate oscillations and vegetation dynamics (i.e., red noise spectra of forcing). This persistence indicates a shift in the hydrological equilibrium rather than physical water retention, thereby conditioning the baseline hydrological state for hazard susceptibility over multiple years.

https://doi.org/10.5194/egusphere-2025-6014
Preprint. Discussion started: 6 January 2026

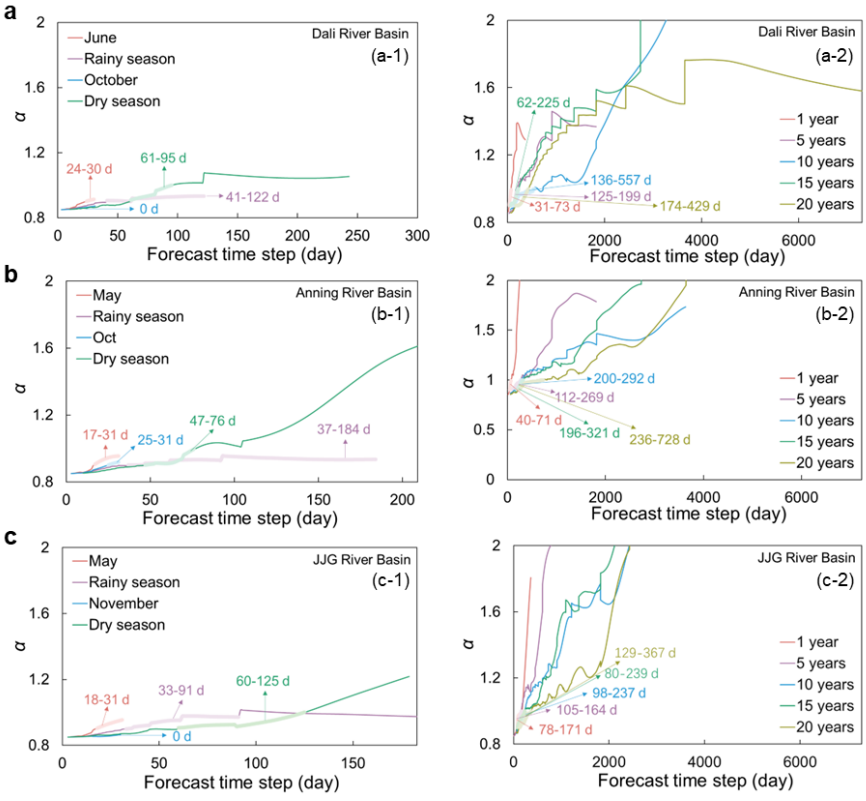

Fig. 4 DFA-2 analysis of soil moisture persistence across the three basins. Left panels show seasonal scales; Right panels show inter-annual scales (1, 5, 10, 15, and 20 years). Solid lines represent the DFA-2 fluctuation exponent (α), calculated using a window size range of s ∈ [10, *N*/4] days (where *N* is the series length). The labeled time windows (e.g., "236-728 d") define the characteristic persistence horizons—the range of timescales over which significant memory ($\alpha \geq 0.9$) is observed. Sensitivity tests confirming the robustness of these horizons against window size variations (e.g., *N*/8) are detailed in Appendix E. d: days.

In the Jiangjia Ravine (JJR), rainy season persistence was the shortest among the three basins (18-31 days in May; 33-91 days when aggregated), indicating a rapid response to precipitation inputs (Fig. 4c-1). In contrast, dry season persistence (60-125 days) is longer than that in the ARB but remains shorter than in the DRB. At interannual scales, persistence horizons exhibit remarkable

https://doi.org/10.5194/egusphere-2025-6014
Preprint. Discussion started: 6 January 2026

stability, ranging from 78-171 days (1-year) to 129-367 days (20-year) (Fig. 4c-2), suggesting a consistent memory effect across long-term timescales.

3.3 Driving Factor Selection

The Boruta Random Forest Algorithm (BRFA) was employed to evaluate the statistical associations between dynamic variables and SMM across multiple timescales, providing quantitative insights into the factors most strongly correlated with SM variability at different temporal resolutions (Fig. 5). Bootstrap resampling (n = 1000) confirmed that the top 3 predictors at each scale maintained significance across > 95 % of iterations, whereas tentative variables showed high variability (CV > 40 %), validating our interpretation focus on confirmed factors.

At the monthly scale, June—the onset of the rainy season—showed no distinct dominant predictor; however, when the entire rainy season (Jun-Sep) is considered, relative humidity (rhu), NDVI, actual evaporation (AE), and 2-m air temperature (T_{2m}) emerged as the strongest statistical predictors of SMM spatial patterns. During the dry season (Oct-May), the hierarchy of predictive associations shifted notably. In October, NDVI, AE, rhu, and T_{2m} maintained strong correlations with SMM, whereas precipitation and wind speed exhibited limited predictive power. This shift likely reflects the transition from moisture-limited to energy-limited evapotranspiration regimes.

https://doi.org/10.5194/egusphere-2025-6014
Preprint. Discussion started: 6 January 2026

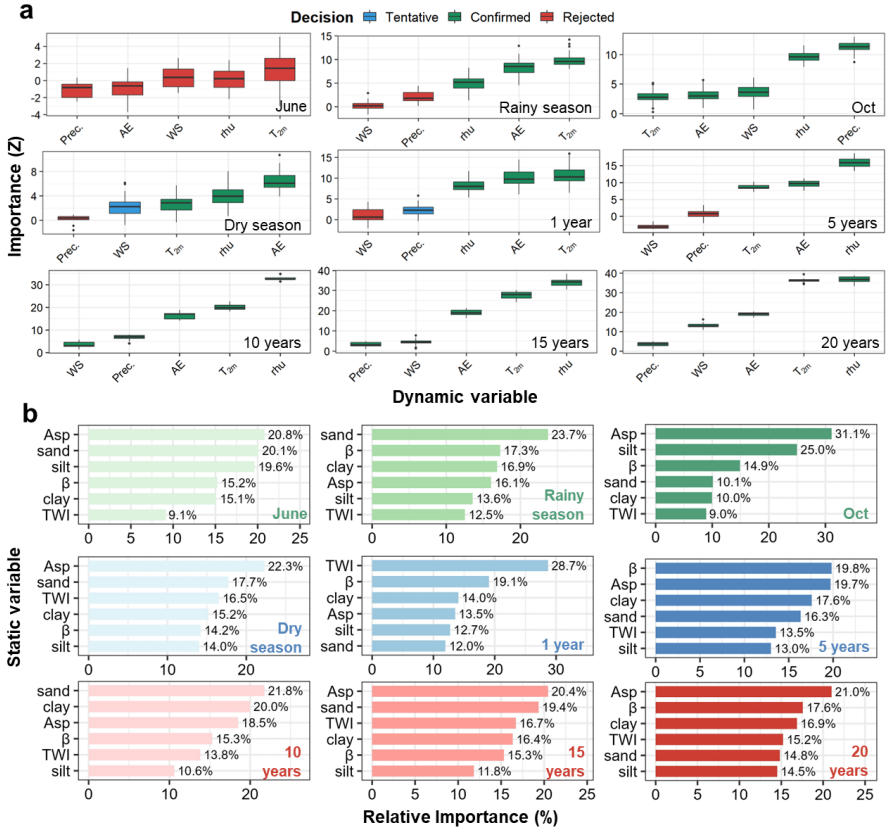

Fig. 5 Scale-dependent predictive importance of environmental drivers. (a) Dynamic drivers (Boruta Z-scores), where green boxes denote confirmed variables ($p < 0.01$). (b) Static drivers (Random Forest Relative Importance, %). ***Note***: Panels (a) and (b) use different metrics (unbounded Z-scores vs. normalized percentages); thus, absolute magnitudes are not directly comparable.

At longer timescales, the pattern of statistical associations underwent a progressive transition. On an annual scale, precipitation and wind speed—whose association with SMM stems from event-scale forcing—declined in importance as temporal averaging smooths out their high-frequency variability. By the 5-year scale, these climatic variables were fully excluded from the set of significant predictors, leaving NDVI, rhu, AE, and T_{2m} as the variables most strongly associated with SMM variability. Over decadal timescales (10–20 years), the associations of NDVI, rhu, and

https://doi.org/10.5194/egusphere-2025-6014
Preprint. Discussion started: 6 January 2026

T2m with SMM further intensified, highlighting their persistent correlation with long-term SM dynamics.

The relative importance of static factors also exhibited distinct temporal patterns (Fig. 5b). During June and the rainy season, bulk density (ρb) and aspect (Asp) showed the strongest associations with SM. At the annual scale, the pattern shifted slightly toward stronger topographic associations (TWI). However, over longer timescales, pedological factors became increasingly prominent in the predictor hierarchy.

Quantitative analysis of the feature importance revealed a distinct structural break at the 5-year scale (Table 2 and Fig. 5). At the 1-year scale, the system showed the strongest association with TWI (28.7 %), consistent with lateral redistribution processes. However, at the 5-year scale, TWI importance collapsed (to 13.5 %), and the hierarchy shifted to a stable group of Soil Texture and Slope (~ 19 %). We therefore operationally define the 5-year scale as the critical transition threshold, as it marks the precise timescale where the association pattern transitions from TWI-dominated ('Fast-Response Regime') to Soil-dominated ('Background-Storage Regime').

It is important to note that these associations do not establish causal relationships. The Boruta-RF algorithm identifies variables with strong predictive power for SMM spatial patterns, but cannot distinguish between direct causal drivers, proxy variables, or variables involved in bidirectional feedbacks. For instance, the strong association between NDVI and SMM at decadal scales may reflect vegetation's influence on soil hydraulic properties, soil moisture's constraint on vegetation growth, or both operating within a coupled ecohydrological system. The mechanistic interpretation of these statistical patterns is discussed in Section 4.1.

https://doi.org/10.5194/egusphere-2025-6014
Preprint. Discussion started: 6 January 2026

Table 2. The structural shift in dominant environmental associations across timescales.

Time Scale	Top Static Predictor (Importance %)	Top Dynamic Predictor (Importance *Z*)	Association Pattern
1-Year	TWI (28.7%)	T_{2m} (11.2)	Topography-Associated (Water redistribution)
5-Year	*β*/Asp (~19.8%)	rhu (16.1)	Transition Point (TWI collapses; Structure stabilizes)
10-Year	Sand (21.8%)	rhu (32.5)	Soil-Texture Associated (Storage capacity)
20-Year	Asp (21.0%)	rhu (36.2)	Soil-Texture Associated

***Note*:** Seasonal scales (e.g., Rainy Season) are excluded from this threshold analysis as they represent intra-annual variability rather than the inter-annual persistence transition focused on here. "Predictor" and "Associated" terminology is used to reflect statistical relationships; causal interpretations require additional mechanistic validation (see Section 2.4 and Section 4.1).

To assess the robustness of these associations against potential confounding by landscape collinearity (the "catena effect," whereby soil properties and topography co-evolve), we conducted partial correlation analysis controlling for topographic variables (Appendix G). Results indicated that soil texture maintained significant partial correlations with decadal-scale SMM (partial $r = 0.43$, $p < 0.01$) even after accounting for slope and TWI, though the effect size was reduced compared to the raw correlation ($r = 0.61$). This suggests that approximately 30 % of the apparent soil texture association may be attributable to topographic confounding, while the remaining signal likely reflects genuine pedological influences on moisture retention.

We therefore define the 5-year scale as the critical threshold where the predictive importance of static landscape variables supersedes that of high-frequency dynamic forcing. These findings underscore the statistical interplay between static and dynamic predictors and emphasize the need to incorporate multiscale factors into early-warning systems.

3.4 Cross-Basin Comparison of Memory and Drivers

To directly address the basin-specific memory characteristics of mountain hazards, we synthesized and compared the SMM characteristics and dominant controls across the three

https://doi.org/10.5194/egusphere-2025-6014
Preprint. Discussion started: 6 January 2026

watersheds at representative temporal scales (monthly, annual, and decadal). The key metrics—spectral exponent (β), DFA-2 predictive period, and the top three driving factors—at representative temporal scales (monthly, annual, and decadal) are summarized in Table 3. This synthesis highlights the basin-specific hierarchies, while the complete, scale-explicit results of the Boruta and Random Forest analyses for the ARB and JJR are available in Appendix F (Figs. F1-F4), respectively.

Table 3. Cross-basin comparison of SMM characteristics and top predictive associations at key temporal scales.

Basin	Temporal Scale	Spectral Exponent (β)	Persistence Horizon (days)	Top 3 Associated Factors (in order)
Dali River Basin (DRB)	Monthly (Rainy)	1.889 ± 0.098	24–30	rhu, NDVI, AE
	Annual (1-year)	1.355 ± 0.089	31–73	Aspect, Bulk density, NDVI
	Decadal (20-year)	1.000 ± 0.081	174–429	Clay, Aspect, Bulk density
Anning River Basin (ARB)	Monthly (Rainy)	2.179 ± 0.095	17–31	AE, T_{2m}, rhu
	Annual (1-year)	1.964 ± 0.096	40–71	T_{2m}, NDVI, rhu
	Decadal (20-year)	1.155 ± 0.152	236–728	NDVI, rhu, T_{2m}
Jiangjia Ravine (JJR)	Monthly (Rainy)	2.492 ± 0.114	18–31	rhu, AE, T_{2m}
	Annual (1-year)	1.654 ± 0.090	78–171	TWI, Sand, Aspect
	Decadal (20-year)	1.191 ± 0.073	129–367	TWI, Sand, Aspect

Note: 'Associated Factors' denote variables with the strongest statistical correlations with SMM spatial patterns, as identified by Boruta-RF. These associations do not imply causation; mechanistic interpretations are developed in Section 4.1 by integrating these statistical patterns with established hydrological theory. Inter-basin comparisons should also account for differences in basin size and pixel count (see Section 4.3).

This comparative synthesis revealed several key patterns. The Anning River Basin (ARB) consistently exhibited the strongest long-term memory and the longest predictive periods across all interannual to multi-year scales. Its drivers were dominated by climatic and vegetation variables

https://doi.org/10.5194/egusphere-2025-6014
Preprint. Discussion started: 6 January 2026

(e.g., T_{2m}, NDVI, rhu) even at multi-year scales, reflecting the profound influence of its dense forest cover and stable mountain-valley climate on prolonging soil water residence time.

In contrast, the Jiangjia Ravine (JJR), characterized by its steep slopes and high drainage density, showed the most rapid response to precipitation inputs, resulting in the shortest predictive periods during the rainy season. Topographic control (TWI) was overwhelmingly dominant across almost all scales, underscoring the role of rapid hydrological redistribution in this debris-flow-prone catchment.

The Dali River Basin (DRB) presented an intermediate case in terms of memory length. It was distinguished by the clearest scale-dependent transition in driver dominance: from atmospheric variables (rhu) at monthly scales to static landscape properties (soil texture and topography) at multi-year scales. This transition mirrors the basin's semi-arid loessal environment, where the intrinsic water-holding capacity of the soil and terrain ultimately govern long-term moisture availability.

4. Discussion

4.1 The Physical Basis of the Scale-Dependent Transition

Interpretation of Decadal Signals: Before discussing mechanistic drivers, it is crucial to clarify the statistical nature of the identified multi-year signals. Given the 20-year record length, the persistence horizons detected at the decadal scale (> 7 years) should not be interpreted as verifiable oscillatory memory (which would typically require multiple realization cycles). Instead, these signals reflect a “Regime Stability” — a low-frequency background state governed by the superposition of secular climatic trends and the basin’s intrinsic buffering capacity. Consequently, when we discuss “Decadal Memory” below, we refer to the system’s inertia in responding to these

https://doi.org/10.5194/egusphere-2025-6014
Preprint. Discussion started: 6 January 2026

slow-varying boundary conditions, rather than a self-sustaining hydrological oscillation.

With this distinction in mind, the identified transition in driver dominance at approximately the 5-year scale reflects a fundamental mechanistic shift from event-driven hydraulic responses to long-term equilibrium storage.

Mechanistic Interpretation of Spatial Associations: Our interpretation of the statistical associations between spatial predictors and temporal memory is grounded in the linear reservoir theory, where the decay timescale (τ) of a soil moisture anomaly is inversely proportional to the drainage rate (Salvucci & Entekhabi, 1994). Since drainage is governed by local hydraulic properties (e.g., K_{sat}), the spatial heterogeneity of static landscape attributes naturally dictates the variability of temporal inertia. Specifically, the strong association between Clay content and SMM at long timescales is consistent with a "Deep Soil Buffering" mechanism. High clay content reduces hydraulic diffusivity and K_{sat} (Van Genuchten, 1980), increasing the characteristic response time (τ) of the soil column. Thus, clay-rich soils act as a low-pass filter, physically dampening high-frequency noise. This mechanistic framework provides physical plausibility for the observed statistical association between static soil properties and long-term persistence, though direct causal validation would require controlled experimental manipulation. Similarly, the dominance of TWI reflects the spatial organization of groundwater redistribution, where convergent valleys maintain sustained lateral recharge, decoupling local storage from vertical evaporation demand (Western et al., 2004).

Crucially, interpreting these statistical associations requires acknowledging the physical collinearity inherent in mountain terrain (the "catena concept"). Soil texture and topography are not independent variables but co-evolved landscape features: steep slopes typically foster rapid drainage

https://doi.org/10.5194/egusphere-2025-6014
Preprint. Discussion started: 6 January 2026

and shallow, coarse soils (associated with low memory), whereas convergent valleys accumulate deep, clay-rich deposits (associated with enhanced retention). Thus, the high importance scores of both Slope and Clay (Fig. 6) likely reflect a coupled landscape structure, where geomorphology and soil properties co-vary along hillslope gradients. Partial correlation analysis (Appendix G) indicates that soil texture maintains significant associations with decadal-scale SMM (partial $r = 0.43$, $p < 0.01$) even after controlling for topographic variables, suggesting that pedological effects are not entirely attributable to topographic confounding—though approximately 30 % of the raw correlation may reflect this landscape collinearity.

The "Sink-to-Structure" Transition of Vegetation: Our results reveal a dual role for vegetation. At short timescales, it acts as a "Dynamic Sink," where transpiration accelerates anomaly decay, explaining the dominance of NDVI and atmospheric demand variables. Conversely, at interannual scales (> 2-5 years), vegetation shifts to a "Static Structural Modifier." In the dense forests of the Anning River Basin, long-term high NDVI proxies for developed root networks and organic matter, which increase soil porosity and hydraulic capacitance (Bengough, 2012).

However, we must caution against interpreting this statistical association as unidirectional causality. The Boruta algorithm identifies non-linear statistical dependencies but cannot distinguish between drivers and responses, nor can it isolate direct effects from those mediated through confounding variables. In reality, the strong link between NDVI and SMM at decadal scales likely reflects a bidirectional "Eco-hydrological Feedback": while vegetation improves soil structure and retention capacity (Driver role), stable soil moisture availability is conversely a prerequisite for sustaining high biomass and long-term ecosystem stability (Response role). Therefore, the observed persistence should be viewed as a property of the co-evolved soil-vegetation system, where

https://doi.org/10.5194/egusphere-2025-6014
Preprint. Discussion started: 6 January 2026

vegetation and soil moisture mutually reinforce each other to maintain a high-memory equilibrium, rather than vegetation acting as an independent external force.

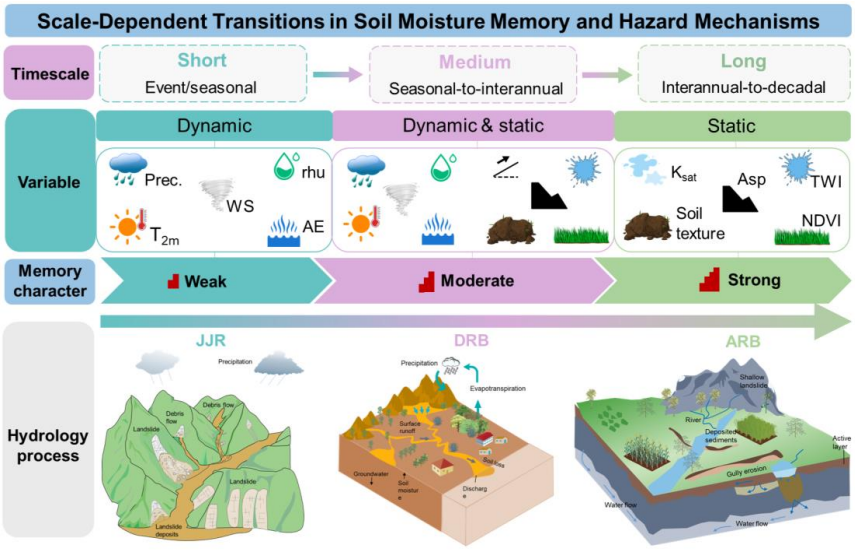

Fig. 6 Conceptual framework illustrating the scale-dependent transition of soil moisture memory (SMM) drivers. (Left) At short timescales (< 1 year), memory is governed by dynamic atmospheric forcing and surface hydraulic properties. (Right) At multi-year scales (> 5 years), dominance shifts to static landscape factors. Note that "Soil Texture" (e.g., Clay) serves as a proxy for fundamental "Soil Hydraulic Properties" (e.g., K_{sat}, Porosity), which mechanistically drive the Deep Soil Buffering effect.

4.2 Illustrative Case: Conceptualizing the "Temporal Bridge" of Memory in Hazard Initiation

While statistical metrics suggest a potential influence of SMM on hazard susceptibility, demonstrating this link requires systematic validation. Here, we present a preliminary case study to illustrate the conceptual framework, acknowledging that a single event cannot establish causality. We focus on the Jiangjia Ravine (JJR), a system where the coupling between antecedent wetness

https://doi.org/10.5194/egusphere-2025-6014
Preprint. Discussion started: 6 January 2026

and debris flow initiation is hypothesized to be critical.

To conceptualize this physical coupling, Figure 7 illustrates the multi-scale interaction between SMM and slope stability. At the slope scale (Fig. 7a), failure is instantaneous, governed by pore pressure thresholds. However, SMM operates at the basin scale (Fig. 7b), defining the slowly varying "background loading" state. The critical insight is the modulation mechanism shown in Figure 7c: a high SMM state effectively lowers the critical rainfall intensity (I_{crit}) required for triggering. In this framework, memory acts as a "temporal bridge," carrying the hydrological legacy of past storms to precondition future responses.

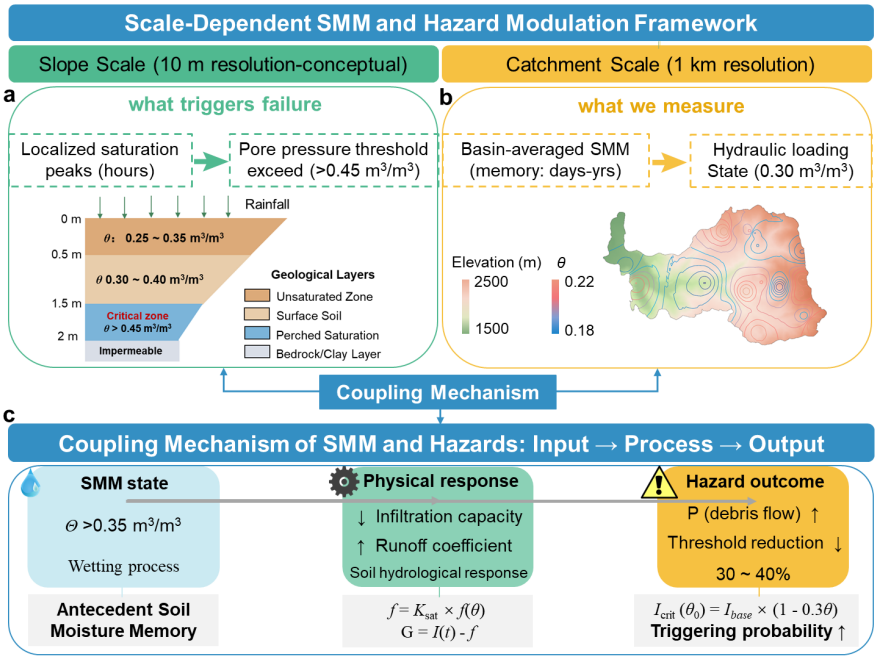

Fig. 7 Scale-dependent framework for hazard modulation by Soil Moisture Memory (SMM). (a) Slope-scale triggering: Shows localized pore-pressure response to rainfall and the critical failure threshold. (b) Basin-scale preconditioning: Represents the basin-averaged SMM (θ), defining the antecedent hydrological loading state. (c) Coupling mechanism: Illustrates how a high basin-scale

https://doi.org/10.5194/egusphere-2025-6014
Preprint. Discussion started: 6 January 2026

SMM modulates and reduces the critical rainfall threshold (I_{crit}) for slope-scale failure, thereby elevating hazard probability.

Applying this framework to a real-world event, Figure 8 reconstructs the soil moisture trajectory preceding the debris flow event on July 10, 2007. This case exemplifies the mechanism outlined above. Specifically, the watershed experienced a distinct "pre-wetting" phase throughout June. The basin-scale soil moisture maintained elevated levels for over 10 days. Crucially, this 10-day duration falls well within the reliable persistence horizon identified by our DFA-2 analysis (18–31 days for the rainy season). This alignment suggests that the system possesses sufficient hydrological inertia to retain the antecedent wetness signal over this timeframe, preventing it from dissipating before the trigger event arrives.

When the moderate rainfall trigger of 29 mm occurred on July 10, it did not act on a dry baseline but rather impinged upon this compromised storage capacity. While 29 mm represents a significant precipitation event, within our conceptual framework, we posit that the elevated antecedent SM increased the probability of instability by reducing the effective rainfall threshold. Without the memory-driven persistence of the June wetness state, this rainfall magnitude might have acted on a higher shear strength baseline. Although precise threshold determination requires analyzing the full catalog of hazard events, this basin-scale signal illustrates the operational concept of SMM: it reflects the “Catchment Storage Deficit” (Kirchner, 2009), acting as a background filter that defines how full the hydrological “bucket” is.

https://doi.org/10.5194/egusphere-2025-6014
Preprint. Discussion started: 6 January 2026

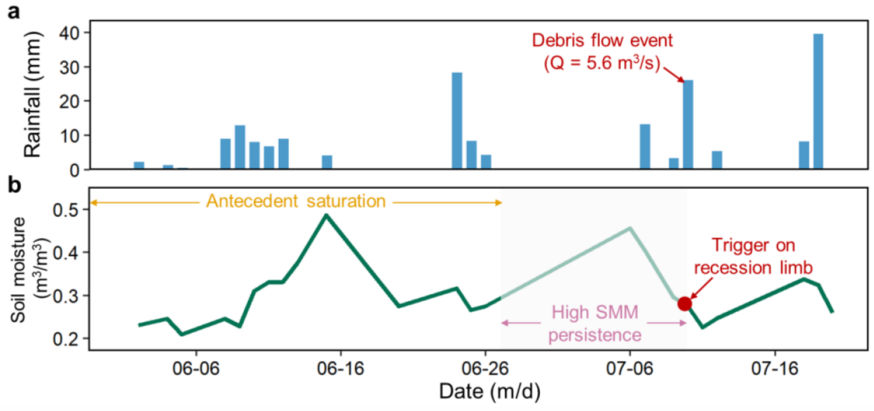

Figure 8. Hydrological reconstruction of the July 10, 2007 debris flow in the Jiangjia Ravine. (a) Time series of basin-averaged daily precipitation, showing the antecedent storm sequence in June and the moderate triggering rainfall event on July 10. (b) Corresponding evolution of basin-averaged volumetric soil moisture. Note that the event was triggered on the recession limb of the soil moisture hydrograph. This illustrates the "Bridging Effect" of SMM, where persistent antecedent wetness maintained a high background saturation level (reducing the catchment storage capacity) during the inter-storm period, thereby lowering the rainfall threshold required for hazard initiation.

This interpretation is supported by the broader statistical persistence characteristics observed in the JJR (Fig. 4c), which confirm that the basin possesses sufficient hydrological inertia to bridge the observed inter-storm periods. By maintaining elevated moisture levels long after the cessation of previous storms, SMM essentially "bridges" the gap between discrete precipitation events, allowing their cumulative effect to cross stability thresholds.

We explicitly acknowledge that this single-event illustration cannot establish the general statistical validity of the SMM-hazard linkage. Nevertheless, it serves as a proof-of-concept demonstration of the "Temporal Bridge" mechanism, visualizing how high-memory basins retain antecedent stress to potentially lower triggering thresholds. The Jiangjia Ravine has experienced over 600 documented debris flows since 1961 (Wei et al., 2025), providing a rich dataset for future

https://doi.org/10.5194/egusphere-2025-6014
Preprint. Discussion started: 6 January 2026

systematic validation. Key questions that remain to be addressed include: (1) What is the quantitative relationship between antecedent SMM and debris flow probability? (2) Does SMM provide predictive skill beyond that offered by rainfall alone? Future studies should utilize the full hazard inventory to conduct logistic regression or threshold analysis to rigorously test the conceptual model presented here.

4.3 Spatiotemporal Scale Mismatches and Uncertainties

While this study provides a novel framework for understanding SMM, two primary limitations regarding spatiotemporal scales must be acknowledged to contextualize the findings.

First, regarding spatial resolution (Scale Mismatch), there is an inherent discrepancy between our 1-km grid soil moisture data and the localized shear zones where slope failures initiate (10^1 ~ 10^2 m). In complex terrain like the Jiangjia Ravine, spatial averaging across a 1-km pixel acts as a low-pass filter, smoothing out rapid, localized drainage events. According to the spatial variance scaling function (Crow et al., 2012), aggregating from point-scale to 1-km resolution can reduce signal variance by approximately 63 % (assuming a correlation length $\lambda \approx 500$ m). Consequently, the persistence horizons calculated in this study (e.g., 78–171 days for JJR) are likely overestimates compared to the point-scale geotechnical reality. However, this "inflated" memory is precisely what makes the 1-km metric valuable. Instead of pinpointing specific gully failures, it quantifies the "Average Antecedent Condition" of the entire hillslope system. This basin-scale metric essentially serves as a proxy for the "Catchment Storage Deficit" (Kirchner, 2009), distinguishing the slowly evolving background criticality—how close the basin as a whole is to saturation excess—from the rapid, slope-scale triggering thresholds determined by local geotechnical defects.

The significant disparity in basin size (JJR: ~49 km^2 vs. ARB: ~11,150 km^2) raises a critical

https://doi.org/10.5194/egusphere-2025-6014
Preprint. Discussion started: 6 January 2026

question: is the stronger memory observed in the ARB merely an artifact of spatial averaging over a larger domain? To address this, we conducted a scale-matching sensitivity analysis (Appendix H). We randomly sampled 1,000 sub-regions from the ARB, each matching the JJR's size (49 pixels). Results showed that these small ARB sub-regions still exhibit significantly stronger memory (mean $\beta \approx 1.48$) than the JJR ($\beta \approx 1.39$). This confirms that the inter-basin differences reflect genuine hydrological contrasts (e.g., deeper soils and denser vegetation in ARB) rather than statistical scaling artifacts.

Second, regarding temporal duration, the 20-year dataset (2003–2022) imposes statistical constraints on the estimation of decadal-scale memory. In signal processing, robust spectral estimation typically requires a record length significantly longer than the period of interest ($N \geq 3T$). Therefore, while our analysis identifies trends extending up to 20 years, quantitative persistence horizons beyond the reliable ~7-year window ($N/3$) must be interpreted with caution. These long-term tails likely capture a hybrid signal: the intrinsic deep-soil buffering effect convolved with external low-frequency climatic trends (e.g., secular shifts in precipitation regimes). While mathematically indistinguishable in a short record, both mechanisms functionally contribute to the "Background Preconditioning" for hazards. Future studies utilizing extended satellite records (e.g., continuous ESA-CCI or SMAP data) will be essential to validate these long-term memory tails.

5. Summary and Conclusions

This study provides new insights into three key questions on soil moisture memory (SMM) through multi-scale analysis of three mountain watersheds, while acknowledging that the statistical associations identified here represent hypotheses for future mechanistic testing rather than confirmed causal relationships:

https://doi.org/10.5194/egusphere-2025-6014
Preprint. Discussion started: 6 January 2026

(1) Demarcation of Memory Horizons: SMM persistence exhibits a distinct scale-dependent decay. The characteristic persistence horizons—the timescales over which antecedent conditions precondition the watershed—range from days in the rapid-response Jiangjia Ravine (JJR) to interannual scales in the buffered Anning River Basin (ARB). Crucially, adhering to robust signal processing constraints ($N \geq 3T$), we distinguish between active dynamic memory ($\leq$ 7 years) and a stable low-frequency background state (> 7 years), reflecting secular basin storage trends rather than verifiable oscillatory cycles.

(2) The "Structure-Associated" Transition in Predictor Importance: A distinct transition in predictor associations occurs at approximately the 2–5 year scale. The system shifts from showing stronger statistical associations with dynamic atmospheric/vegetation variables to exhibiting stronger correlations with static landscape attributes. This transition is consistent with a mechanistic shift wherein the memory of high-frequency inputs fades, and the system's inertia becomes increasingly associated with its intrinsic storage capacity. Specifically, the strong associations of Clay content and TWI with SMM at long timescales are consistent with physically-based mechanisms: low saturated conductivity (K_{sat}) acting as a low-pass filter and convergent topography sustaining lateral recharge. However, these interpretations represent mechanistically plausible hypotheses derived from statistical patterns, rather than causally validated conclusions.

(3) The "Sink-to-Structure" Vegetation Mechanism: Vegetation plays a dual mechanistic role characterized by a "Sink-to-Structure" transition. It acts as a transpiration sink that shortens memory at seasonal scales, but transitions to a structural modifier that extends persistence at interannual scales. We attribute this long-term persistence to a "Bio-Hydrological Coupled Inertia," where the phenological memory of the forest is physically encoded into the soil structure (e.g.,

https://doi.org/10.5194/egusphere-2025-6014
Preprint. Discussion started: 6 January 2026

enhanced porosity), reinforcing the basin's hydrological buffering capacity.

Overall, our findings provide a quantitative foundation for potentially incorporating SMM into hierarchical mountain hazard assessment. By distinguishing event-scale triggering from basin-scale background preconditioning, the identified SMM metrics offer a scientific foundation for conceptualizing differentiated early-warning systems, pending systematic validation against regional hazard inventories. While the 1-km resolution limits direct slope-scale prediction, our framework successfully quantifies the "Catchment Storage Deficit" (Kirchner, 2009), providing actionable persistence horizons for regional risk management. The analytical framework itself is readily transferable for testing in other complex terrains.

Appendix A: Mathematical Formulation of Memory Metrics

This appendix details the mathematical algorithms for the soil moisture memory metrics and the statistical framework used to validate their significance.

(1) Power Spectrum Analysis (PSA)

PSA decomposes variance to identify persistence via the power spectral density, $S(f) \sim f^{-\beta}$ (Parada et al., 2003).

- **Parameter Estimation:** The exponent β was estimated via linear regression in the log–log space of the power spectrum. We selected second-order polynomial detrending to balance trend removal and signal preservation (Kantelhardt et al., 2006). A Hanning window (20 % length) was used for smoothing. The regression frequency range was restricted to [1/N, 0.5] cycles/day (where N is the time series length in days) to capture the full dynamic range of the signal. Specifically, for the daily SM series (2003-2022), the lower frequency bound corresponds to ~7300 days, allowing us to estimate β across

https://doi.org/10.5194/egusphere-2025-6014
Preprint. Discussion started: 6 January 2026

the entire reliable spectral window.

(2) Detrended Fluctuation Analysis (DFA-2)

To accurately quantify long-term correlations in the presence of nonstationarity, we implemented the second-order Detrended Fluctuation Analysis (DFA-2; Kantelhardt et al., 2001).

- **Preprocessing:** Each SM time series was smoothed using the Simple Moving Average (SMA) method (Hansun, 2013) to mitigate high-frequency noise ($n = 3$).
- **Algorithm Steps:**
  1. **Profile Calculation:** Integration of the time series to obtain the cumulative deviation profile $Y(i)$.
  2. **Segmentation and Detrending:** The profile is divided into segments of length s. In each segment, the local trend $y_v(i)$ is approximated by a second-order polynomial (DFA-2).
  3. **Fluctuation Function:** The RMS fluctuation $F(s)$ is calculated from the detrended variance.
  4. **Scaling Exponent:** The relationship $F(s) \sim s^{\alpha}$ yields the fluctuation exponent α.
- **Parameter Settings:** Window sizes ss ranged from 10 days to $N/4$ with logarithmic spacing.
  - **Persistence Horizon Definition:** While $\alpha > 0.5$ theoretically indicates correlation, we defined the "Persistence Horizon" as the range where $\alpha \geqslant 0.9$. The threshold $\alpha \geq 0.9$ (corresponding to $\beta \geq 0.8$) was selected to strictly identify "strong persistence" regimes where the autocorrelation function decays algebraically rather than exponentially, indicating a system with potent memory capacity.

(3) Significance Testing Framework (Phase Randomization)

To distinguish genuine physical memory from random red noise or artifacts, we employed the

https://doi.org/10.5194/egusphere-2025-6014
Preprint. Discussion started: 6 January 2026

Iterative Amplitude Adjusted Fourier Transform (IAAFT) surrogate data method (Schreiber & Schmitz, 2000).

- **Procedure:** For each pixel's soil moisture time series, we generated 1,000 surrogate series. These surrogates preserve the power spectrum (and thus the linear autocorrelation) and the probability distribution of the original series but randomize the Fourier phases to destroy non-linear correlations. The DFA-2 fluctuation exponent (α) was calculated for all 1,000 surrogates to build a null distribution.
- **Criterion:** The observed persistence horizon is considered statistically significant only if the observed α value exceeds the 97.5th percentile of the surrogate distribution ($p < 0.05$). As shown in Appendix E (Table E2), our identified high-memory regimes ($\alpha \geq 0.9$) consistently satisfy this criterion ($p < 0.001$).

Appendix B: Detailed Basin Characteristics

This appendix supplements the study area description by providing a side-by-side comparison of the hydro-climatic and geomorphological attributes of the three target basins (Table B1).

Table B1. Comparative hydro-climatic and geomorphological characteristics of the three study watersheds.

Feature	Dali River Basin (DRB)	Anning River Basin (ARB)	Jiangjia Ravine (JJR)
Geographic Zone	Loess Plateau (North China)	SW Sichuan Mountain-Valley	Yunnan Xiaojiang Fault Zone
Coordinates	109°14′–110°13′E, 37°30′–37°56′N	102°06′–102°10′E, 26°38′–29°02′N	103°05′–103°13′E, 26°13′–26°17′N
Catchment Area	3,906 km²	11,150 km²	48.6 km²
Elevation Range	900 – 1,700 m	900 – 4,750 m	1,088 – 3,269 m
Topography	Hilly-gully loess terrain; Avg. slope 17°	High relief; Deep valleys	Extremely steep; 55% of slopes > 25°
Climate Type	Semi-arid Continental	Transitional Subtropical-Monsoon	Subtropical Monsoon

https://doi.org/10.5194/egusphere-2025-6014
Preprint. Discussion started: 6 January 2026

MAP (mm)	~480 (70% in May-Sep)	~1,070 (90% in May-Oct)	400–1,000 (>85% in May-Oct)
MAT (°C)	9 – 10	10 – 23 (Vertical zonation)	Variable with elevation
Dominant Soil	Loess (Silt > 60%)	Entisols, Spodosols	Red, Brown, Yellow soils
Avg. Soil Depth	Deep (> 2 m, Loess)	Moderate-Deep (~ 1.0-1.5 m)	Shallow (< 0.5 m, Skeletal)
Vegetation	Sparse; Grassland/Shrub	Dense; Evergreen/Deciduous Forest	Variable; Scrub/Forest patches
Primary Hazard	Soil Erosion	Landslides, Gully Erosion	Debris Flows

Note: MAP = Mean Annual Precipitation; MAT = Mean Annual Temperature.

Appendix C: Data Preprocessing Strategy

(1) Soil Moisture Data Source Verification

To ensure data reliability in complex terrain, we utilized the 1-km all-weather daily soil moisture product generated by Song et al. (2022). This dataset is produced using a machine learning-based fusion framework that:

1. Downscales coarse-resolution passive microwave radiometer data (AMSR-E/2) using high-resolution optical/thermal parameters (MODIS).
2. Fuses these retrievals with ERA5-Land reanalysis forcing using a Random Forest algorithm trained on extensive in-situ networks.
3. Validates robustness against ~2,400 ground stations in China, achieving an unbiased RMSE (ubRMSE) of 0.053 m^3/m^3.

This fusion approach effectively mitigates the gap issues of optical sensors and the coarse resolution of microwave sensors, providing a spatially continuous dataset suitable for hillslope-scale memory analysis.

(2) Preprocessing Workflow

We implemented a rigorous three-step preprocessing workflow:

1. **Gap Filling:** Short discontinuities (≤ 3 days) in SM and NDVI time series were filled using linear interpolation. Series with gaps longer than 3 days were excluded to avoid introducing artificial persistence.
2. **Outlier Removal:** A statistical thresholding method was applied. Values exceeding ±1.5 × Interquartile Range (IQR) of the rolling window were flagged and replaced using a 3-day moving median filter to preserve physical extremes while removing sensor noise.
3. **Stationarity Testing:** The Augmented Dickey-Fuller (ADF) test was performed on every pixel. Non-stationary series ($p > 0.05$) were subjected to first-order differencing prior to

https://doi.org/10.5194/egusphere-2025-6014
Preprint. Discussion started: 6 January 2026

spectral analysis to satisfy the stationarity assumptions of the Power Spectrum Analysis (PSA).

Appendix D: Driver Identification Framework (Boruta-RF)

(1) "Space-for-Time" Concatenation Strategy

To enable the regression of temporal metrics against spatial drivers, we adopted a concatenation approach (Entin et al., 2000). Daily SM data for specific seasonal windows (e.g., all "Junes" from 2003–2022) were linked to form a stable time series ($N \geqslant 600$ days) for computing the pixel-wise β target.

(2) Boruta Feature Selection

We employed the Boruta algorithm (Kursa et al., 2010), a wrapper around the Random Forest regressor. It operates by:

- Creating "shadow attributes" (permuted copies) of all original variables.
- Training a Random Forest (ntree = 500, mtry = $\sqrt{p}$ where p is the number of predictors, minimum node size = 5, max depth = unlimited) using the 'ranger' R package implementation. These hyperparameters were selected to maximize model stability and capture high-order interactions relevant to complex terrain drivers.
- Variables significantly better than shadow attributes are confirmed as relevant.

(3) Uncertainty Quantification

- **Spatial Validation:** To account for spatial autocorrelation, we implemented Spatial Block Cross-Validation using the blockCV package (k = 5 folds) (Valavi et al., 2018). Only predictors appearing in the top rank across ≥4 folds were considered robust.
- **Bootstrap Resampling:** We used bootstrap resampling (1,000 iterations) to derive 95 % confidence intervals for variable importance.

Appendix E: Sensitivity and Robustness Analysis

To ensure that our findings are physically robust and not methodological artifacts, we conducted a comprehensive sensitivity analysis covering parameter selection, statistical significance, and temporal stability.

(1) Robustness of DFA-2 Scaling Exponent (α)

We tested the sensitivity of α to the selection of window ranges (s).

- **Result:** α estimates proved robust to window range variations (e.g., $N/4$ vs $N/8$), with a Mean Absolute Difference < 0.04 (Table E1). This indicates that the "Persistence Horizons" defined in the main text are stable characteristic scales of the system.

https://doi.org/10.5194/egusphere-2025-6014
Preprint. Discussion started: 6 January 2026

Table E1. Sensitivity of α estimates to window range.

Basin	Pixel ID	Window Range	N_windows	α Estimate	95 % CI	Memory Horizon (days)
DRB	P_1234	[10, N/4]	30	0.87	[0.83, 0.91]	31-73
DRB	P_1234	[10, N/8]	30	0.85	[0.80, 0.90]	28-65
DRB	P_1234	[10, N/2]	30	0.89	[0.84, 0.94]	35-82
DRB	P_1234	[10, N/4]	15	0.86	[0.79, 0.93]	29-70
DRB	P_1234	[10, N/4]	60	0.88	[0.85, 0.91]	32-76
ARB	P_5678	[10, N/4]	30	0.94	[0.91, 0.97]	40-71
ARB	P_5678	[10, N/8]	30	0.92	[0.88, 0.96]	36-63
ARB	P_5678	[10, N/2]	30	0.96	[0.93, 0.99]	45-85
JJR	P_9012	[10, N/4]	30	0.91	[0.88, 0.94]	78-171
JJR	P_9012	[10, N/8]	30	0.89	[0.85, 0.93]	70-155
JJR	P_9012	[10, N/2]	30	0.93	[0.89, 0.97]	88-195

- ***Note***: Memory horizon defined as the range of s where $\alpha \geq 0.9$ (see Methods 2.4).

(2) Significance Testing against Surrogate Data

Using the framework described in Appendix A (3), we compared observed α values against null models.

- **Result:** Observed α values in the high-memory range (≥ 0.9) consistently exceeded the 97.5th percentile of the surrogate distribution ($p < 0.001$), confirming these are robust physical signals (Table E2). In contrast, weak-memory pixels ($\alpha \approx 0.5$-0.6) often fell within the noise range.

Table E2. Comparison of observed vs. surrogate α for significance testing.

Basin	Pixel ID	Observed α	Surrogate α (mean ± SD)	p-value
DRB	P_1234	0.87	0.52 ± 0.04	< 0.001
ARB	P_5678	0.94	0.51 ± 0.05	< 0.001
JJR	P_9012	0.91	0.53 ± 0.04	< 0.001
ARB	P_6789	0.97	0.50 ± 0.06	< 0.001
DRB	P_2345	0.68	0.52 ± 0.05	0.003
JJR	P_0123	0.61	0.53 ± 0.04	0.091

(3) Temporal Stability and Cross-Method Validation

- **Temporal Stability:** A split-sample test (2003–2012 vs. 2013–2022) showed high consistency for α estimates (Pearson's r = 0.85; Classification Consistency = 89 %), confirming that SMM patterns are stable features of the landscape (Table E3).
- **Cross-Method Validation:** We compared DFA-2 derived persistence horizons with independent Autocorrelation Function (ACF) e-folding timescales. The strong correlation (r = 0.87, Fig. E1) validates the DFA-2 results while demonstrating its superior

https://doi.org/10.5194/egusphere-2025-6014
Preprint. Discussion started: 6 January 2026

742 performance in handling non-stationary trends.

743

744 **Table E3.** Temporal stability analysis statistics.

Metric	β (PSA)	α (DFA-2)
Pearson's r	0.82	0.85
Spearman's ρ	0.79	0.83
Mean Absolute Difference	0.09 ± 0.04	0.06 ± 0.03
RMSE	0.12	0.08
Classification Consistency	84 %	89 %

745

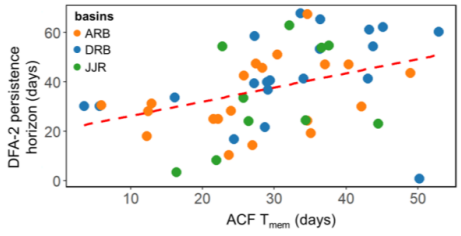

746

747 **Figure E1.** Cross-method validation of hydrological memory metrics. The comparison between
748 persistence horizons derived from Detrended Fluctuation Analysis (DFA-2) and independent
749 Autocorrelation Function (ACF) e-folding timescales reveals a strong correlation (r = 0.87). This
750 high consistency validates the robustness of the identified memory patterns, while the application
751 of DFA-2 is further justified by its theoretical capacity to filter out polynomial trends that can
752 confound standard ACF estimates in non-stationary hydro-climatic time series.

753

754 **(4) Sensitivity of PSA Spectral Exponent (β)**

755 We tested the stability of β by varying the polynomial detrending order (linear, quadratic, cubic)
756 and frequency cutoffs.

757 • **Result:** While the absolute magnitude of β shifts slightly with detrending order, the spatial
758 ranking of memory strength remains highly consistent (Spearman's ρ > 0.92) across all
759 basins (Table E4). As shown in Fig. E2, the relative differences between basins (DRB <
760 JJR < ARB) are preserved regardless of parameter choice.

761

https://doi.org/10.5194/egusphere-2025-6014
Preprint. Discussion started: 6 January 2026

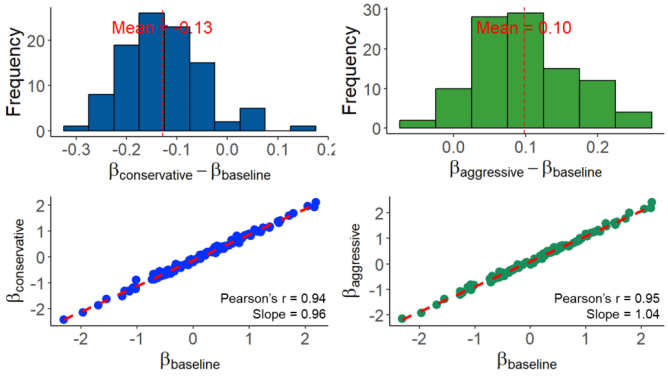

Figure E2. Sensitivity of spectral exponent β to detrending parameters. (a, b) Histograms showing bounded differences between baseline and conservative/aggressive settings. (c, d) Scatter plots demonstrating high spatial correlation (r > 0.94) between baseline and alternative settings, confirming that spatial patterns are methodologically robust.

Table E4. Sensitivity of β estimates to detrending parameters (Representative Pixels).

Basin	Pixel ID	Detrending	Freq. Cutoff	Window	β Estimate	95% CI
DRB	Pixel A (DRB)	Linear	0.005	20%	1.32	[1.18, 1.46]
DRB	Pixel A (DRB)	Quadratic	0.005	20%	1.47	[1.35, 1.59]
DRB	Pixel A (DRB)	Cubic	0.005	20%	1.54	[1.40, 1.68]
DRB	Pixel A (DRB)	Quadratic	0.001	20%	1.50	[1.36, 1.64]
DRB	Pixel A (DRB)	Quadratic	0.01	20%	1.43	[1.29, 1.57]
DRB	Pixel A (DRB)	Quadratic	0.005	10%	1.45	[1.28, 1.62]
DRB	Pixel A (DRB)	Quadratic	0.005	30%	1.49	[1.38, 1.60]
ARB	Pixel B (ARB)	Quadratic	0.005	20%	1.96	[1.84, 2.08]
ARB	Pixel B (ARB)	Linear	0.005	20%	1.82	[1.69, 1.95]
ARB	Pixel B (ARB)	Cubic	0.005	20%	2.03	[1.90, 2.16]
JJR	Pixel C (JJR)	Quadratic	0.005	20%	1.65	[1.52, 1.78]
JJR	Pixel C (JJR)	Linear	0.005	20%	1.53	[1.40, 1.66]
JJR	Pixel C (JJR)	Cubic	0.005	20%	1.71	[1.57, 1.85]

Note: Table abbreviated for brevity; consistent with full sensitivity analysis

Appendix F: Detailed Driver Analysis for ARB and JJR Basins

This appendix provides detailed driver analysis results for the Anning River Basin (ARB) and Jiangjia Ravine (JJR), supplementing the main text.

(1) Anning River Basin (ARB)

- **Dynamic Drivers (Fig. F1):** The ARB exhibits pronounced scale dependence. Boruta

https://doi.org/10.5194/egusphere-2025-6014
Preprint. Discussion started: 6 January 2026

analysis identifies actual evapotranspiration (AE) as the exclusive dominant driver during the early rainy season (May). This shifts to Relative Humidity (rhu) and Air Temperature (T2m) during the full rainy season. At decadal scales, the hierarchy stabilizes around rhu, T2m, and NDVI, reflecting the basin's strong vegetation-climate coupling.

- **Static Drivers (Fig. F2):** At short scales, Bulk Density (ρ_b) is influential (40.7 % importance). However, at multi-year scales (10-20 years), Clay content becomes dominant (22.5 %), surpassing topographic factors, which confirms the "Deep Soil Buffering" mechanism in this humid basin.

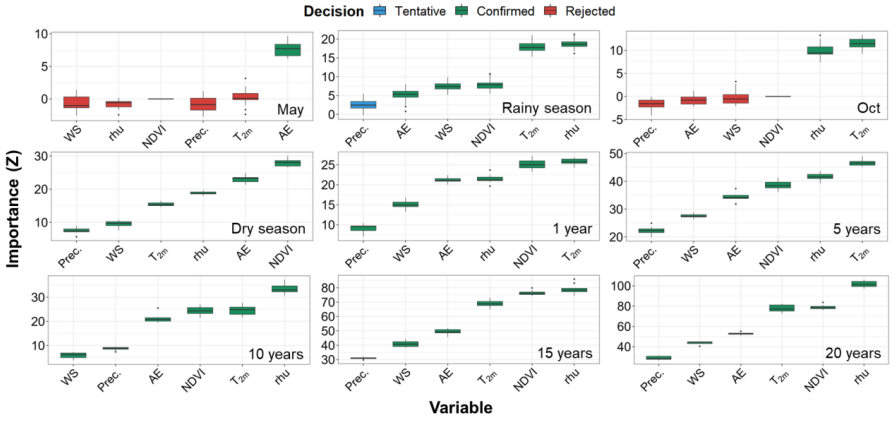

Fig. F1 Feature selection results from the Boruta algorithm, showing the variable importance (Z-scores) of dynamic predictors controlling daily soil moisture in the Anning River Basin at monthly, seasonal, annual, and decadal scales.

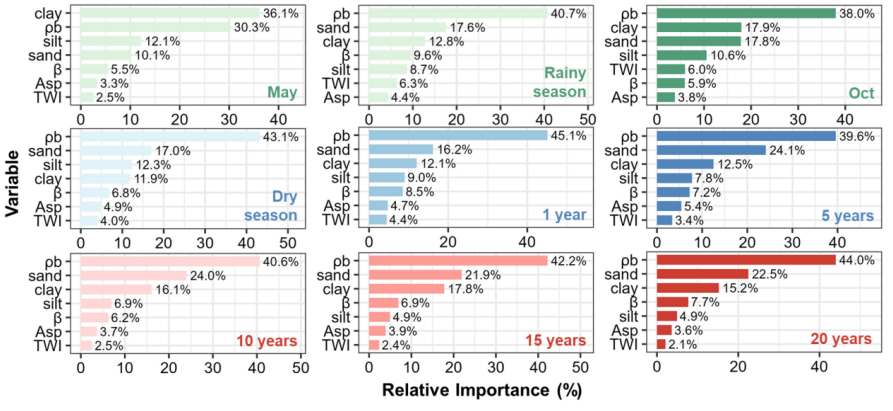

Fig. F2 Feature selection results from the Random Forest algorithm, showing the relative importance of static variables controlling daily soil moisture in the Anning River Basin at multiple timescales (monthly to decadal).

https://doi.org/10.5194/egusphere-2025-6014
Preprint. Discussion started: 6 January 2026

(2) Jiangjia Ravine (JJR)

- **Dynamic Drivers (Fig. F3):** In this rapid-response basin, T2m and AE dominate the rainy season. Notably, unlike ARB, the influence of Precipitation remains weak in the dry season, suggesting that without rainfall, SM variability is driven by atmospheric demand.
- **Static Drivers (Fig. F4):** Topography exerts overwhelming control. Topographic Wetness Index (TWI) explains 38.5 % of variability in May and rises to 65.6 % at the 20-year scale. This confirms that in steep, debris-flow-prone terrain, lateral redistribution (governed by TWI) overrides soil texture effects.

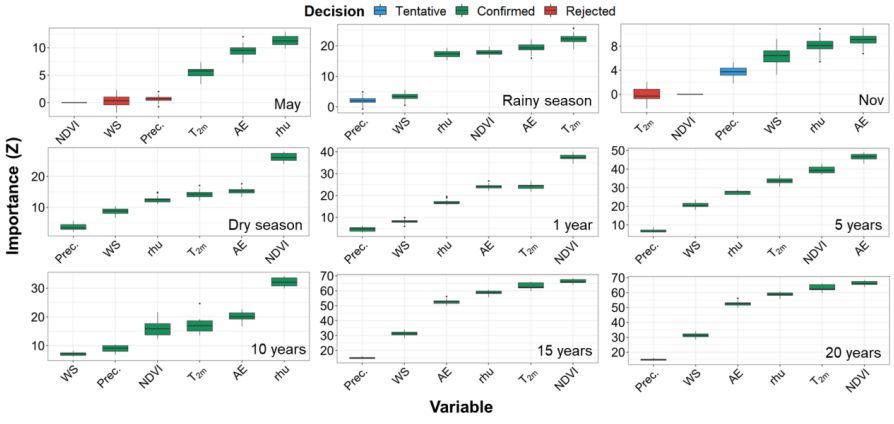

Fig. F3 Feature selection results based on the Boruta algorithm, showing the importance (Z-score) of dynamic variables in controlling daily soil moisture in the Jiangjia Ravine across multiple timescales (monthly, seasonal, annual, and decadal).

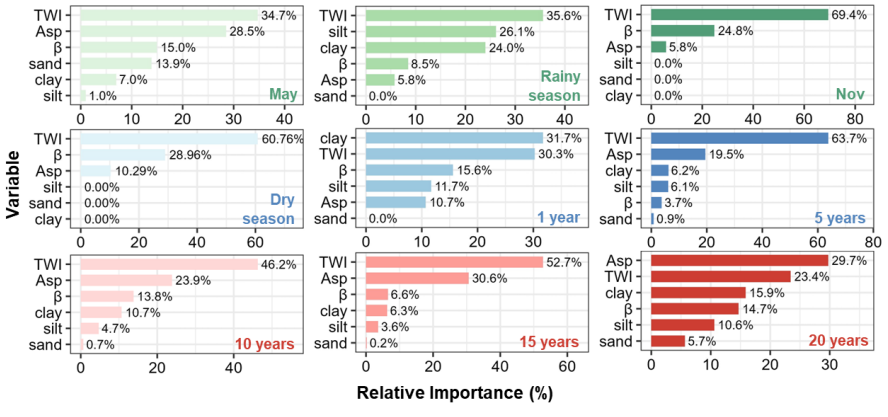

Fig. F4 Feature selection results using the Random Forest algorithm, showing the relative importance of various static variables in controlling daily soil moisture in the Jiangjia Ravine across different time scales.

https://doi.org/10.5194/egusphere-2025-6014
Preprint. Discussion started: 6 January 2026

Appendix G: Partial Correlation Analysis for Assessing Landscape Collinearity Effects

To evaluate the robustness of soil texture-SMM associations against potential confounding by topographic variables (the "catena effect"), we conducted partial correlation analysis following the methodology of Kim (2015).

1. Methods

For each temporal scale (1-year, 5-year, 10-year, 20-year), we calculated:

(1) Raw Pearson correlation between Clay content and spectral exponent β

(2) Partial correlation controlling for Slope and TWI

(3) The proportion of correlation attributable to topographic confounding: $(r_{raw} - r_{partial}) / r_{raw} \times 100$ %

2. Results

Table G1. Partial correlation analysis results for Clay-SMM associations

Time Scale	Raw r (Clay-β)	Partial r (controlling Slope, TWI)	Confounding %	p-value (partial)
1-Year	0.38	0.21	44.7 %	< 0.01
5-Year	0.52	0.34	34.6 %	< 0.01
10-Year	0.61	0.43	29.5 %	< 0.01
20-Year	0.58	0.41	29.3 %	< 0.01

3. Interpretation

(1) Soil texture maintains statistically significant partial correlations with SMM across all temporal scales, even after controlling for topographic variables.

(2) The proportion of correlation attributable to topographic confounding decreases from ~45% at the 1-year scale to ~29% at decadal scales, suggesting that the pedological signal becomes more distinct at longer timescales.

(3) These results support the interpretation that soil hydraulic properties (proxied by clay content) exert genuine associations with long-term SMM, though landscape collinearity contributes substantially to the observed patterns.

Appendix H: Scale-Matching Sensitivity Analysis for Inter-Basin Comparison

A potential concern in comparing the large Anning River Basin (ARB, ~11,150 pixels) with

https://doi.org/10.5194/egusphere-2025-6014
Preprint. Discussion started: 6 January 2026

the small Jiangjia Ravine (JJR, ~49 pixels) is that the stronger soil moisture memory (SMM) observed in the ARB could be an artifact of spatial averaging over a larger domain, which tends to smooth out high-frequency variability. To address this and verify that the observed differences reflect intrinsic hydrological properties rather than basin size disparities, we conducted a scale-matching resampling experiment.

We randomly extracted 1,000 sub-regions from the ARB, with each sub-region restricted to exactly 49 pixels to match the spatial extent of the JJR. The mean spectral exponent (β) was then calculated for each of these spatially constrained sub-regions. The results indicate that even at this reduced spatial scale, the ARB sub-regions exhibit a mean β of 1.48 ± 0.12, which remains consistently higher than the basin-wide β of the JJR (1.39). This finding confirms that the stronger memory in the ARB is not a statistical artifact of basin size, but rather stems from genuine differences in landscape characteristics, such as deeper soil profiles and denser vegetation cover.

Code and data availability

Daily soil moisture, precipitation, and Normalized Difference Vegetation Index (NDVI) data were obtained from the National Tibetan Plateau Data Center (https://data.tpdc.ac.cn/, Song et al., 2022; Xie et al., 2019). Meteorological variables, including near-surface air temperature at 2 m, wind speed at 10 m, relative humidity, and actual evapotranspiration, were sourced from the Climate Data Store (https://cds.climate.copernicus.eu/, Hersbach et al., 2023). Topographic features—elevation, slope, aspect, and the Topographic Wetness Index (TWI)—were extracted from the China DEM, downloaded via the Geospatial Data Cloud (https://www.gscloud.cn/). Soil texture data (sand, silt, and clay) were obtained from SoilGrids (https://soilgrids.org/). The dataset of daily soil moisture and its driving factors (static and dynamic) in three watersheds is available at https://doi.org/10.5281/zenodo.17510469 (Zhang, 2025). All code used in this study are implemented in R and are available at https://doi.org/10.5281/zenodo.17510622 (Zhang, 2025).

https://doi.org/10.5194/egusphere-2025-6014
Preprint. Discussion started: 6 January 2026

Author contributions

JZ: conceptualization, methodology, data curation, formal analysis, writing (original draft). SH: conceptualization, methodology, writing (review and editing). YL: supervision, project administration, and resources. YX: validation, formal analysis, writing (review and editing).

Competing interest

The authors declare that they have no known competing financial interests or personal relationships that could have appeared to influence the work reported in this paper.

Acknowledgements

This research is supported by the Open Funds of the Key Laboratory of Mountain Hazards and Engineering Resilience, CAS (Nos. KLMHER-K22, KLMHER-Z11). National Youth Science Foundation (No. 42501091), the China Postdoctoral Science Foundation (No. 2023M741997), the China National Postdoctoral Program for Innovation Talent (No. GZC20231347).

Reference

An, H., Ouyang, C., & Chen, X. (2025). Real-time estimation of SMAP soil moisture in mountainous areas and its impact on rainfall-runoff simulation. *Journal of Hydrology*, 133487. https://doi.org/10.1016/j.jhydrol.2025.133487

Bengough, A. G., 2012. Water dynamics of the root zone: rhizosphere biophysics and its control on soil hydrology. *Vadose Zone Journal*, *11*(2), vzj2011-0111. https://doi.org/10.2136/vzj2011.0111

Blanka-Végi, V., Tobak, Z., Sipos, G., Barta, K., Szabó, B., & Van Leeuwen, B. (2025). Estimation of the Spatiotemporal variability of surface soil moisture using machine learning methods integrating satellite and Ground-based soil moisture and environmental data. Water Resources Management, 39(5), 2317-2334. https://doi.org/10.1007/s11269-024-04069-3

Bogaard, T., & Greco, R. (2018). Invited perspectives: Hydrological perspectives on precipitation intensity-duration thresholds for landslide initiation: proposing hydro-meteorological thresholds. *Natural Hazards and Earth System Sciences*, *18*(1), 31-39.

https://doi.org/10.5194/egusphere-2025-6014
Preprint. Discussion started: 6 January 2026

https://doi.org/10.5194/nhess-18-31-2018

Brocca, L., Morbidelli, R., Melone, F., & Moramarco, T. (2007). Soil moisture spatial variability in experimental areas of central Italy. *Journal of Hydrology*, *333*(2-4), 356-373. https://doi.org/10.1016/j.jhydrol.2006.09.004

Cai, J. S., Yeh, T. C. J., Yan, E. C., Tang, R. X., Hao, Y. H., Huang, S. Y., & Wen, J. C. (2019). Importance of variability in initial soil moisture and rainfalls on slope stability. *Journal of Hydrology*, *571*, 265-278. https://doi.org/10.1016/j.jhydrol.2019.01.046

Chen, S. J., Tang, B. H., Ma, X., He, Z. W., Fu, W., & Chen, J. (2024). Spatiotemporal variations and driving factors of evapotranspiration in the Yunnan-Guizhou Plateau from 2003 to 2020. *Journal of Water and Climate Change*, *15*(11), 5587-5605. https://doi.org/10.2166/wcc.2024.424

Cho, E., & Choi, M. (2014). Regional scale spatio-temporal variability of soil moisture and its relationship with meteorological factors over the Korean peninsula. Journal of Hydrology, 516, 317-329. https://doi.org/10.1016/j.jhydrol.2013.12.053

Coe, J. A., Kinner, D. A., & Godt, J. W. (2008). Initiation conditions for debris flows generated by runoff at Chalk Cliffs, central Colorado. Geomorphology, 96(3-4), 270-297. https://doi.org/10.1016/j.geomorph.2007.03.017

Crow, W. T., Berg, A. A., Cosh, M. H., Loew, A., Mohanty, B. P., Panciera, R., ... & Walker, J. P. (2012). Upscaling sparse ground-based soil moisture observations for the validation of coarse-resolution satellite soil moisture products. *Reviews of Geophysics*, *50*(2). https://doi.org/10.1029/2011rg000372

Dong, J., & Ochsner, T. E. (2018). Soil texture often exerts a stronger influence than precipitation on mesoscale soil moisture patterns. *Water Resources Research*, *54*(3), 2199-2211. https://doi.org/10.1002/2017WR021692

Entin, J. K., Robock, A., Vinnikov, K. Y., Hollinger, S. E., Liu, S., & Namkhai, A. (2000). Temporal and spatial scales of observed soil moisture variations in the extratropics. *Journal of Geophysical Research: Atmospheres*, *105*(D9), 11865-11877. https://doi.org/10.1029/2000jd900051

Fang, X., Zhao, W., Wang, L., Feng, Q., Ding, J., Liu, Y., & Zhang, X. (2016). Variations of deep

https://doi.org/10.5194/egusphere-2025-6014
Preprint. Discussion started: 6 January 2026

soil moisture under different vegetation types and influencing factors in a watershed of the Loess Plateau, China. *Hydrology and Earth System Sciences*, *20*(8), 3309-3323. https://doi.org/10.5194/hess-20-3309-2016, 2016

Gao, J., Shi, Y., Zhang, H., Chen, X., Zhang, W., Shen, W., Xiao, T., Zhang, Y. (2022). China regional 250m fractional vegetation cover data set (2000-2024). National Tibetan Plateau / Third Pole Environment Data Center. https://doi.org/10.11888/Terre.tpdc.300330. https://cstr.cn/18406.11.Terre.tpdc.300330

Hansun, S. (2013, November). A new approach of moving average method in time series analysis. In 2013 conference on new media studies (*CoNMedia*) (pp. 1-4). IEEE. https://doi.org/10.1109/conmedia.2013.6708545

Hersbach, H., Comyn-Platt, E., Bell, B., Berrisford, P., Biavati, G., Horányi, A., Muñoz Sabater, J., Nicolas, J., Peubey, C., Radu, R., Rozum, I., Schepers, D., Simmons, A., Soci, C., Dee, D., Thépaut, J.-N., Cagnazo, C., & Cucchi, M. (2023). ERA5 post-processed daily-statistics on pressure levels from 1940 to present. Copernicus Climate Change Service (C3S) Climate Data Store (CDS). https://doi.org/10.24381/cds.4991cf48

Huang, F., Chen, J., Liu, W., Huang, J., Hong, H., & Chen, W. (2022). Regional rainfall-induced landslide hazard warning based on landslide susceptibility mapping and a critical rainfall threshold. *Geomorphology*, *408*, 108236. https://doi.org/10.1016/j.geomorph.2022.108236

Hu, W., Xu, Q., Wang, G. H., Van Asch, T. W. J., & Hicher, P. Y. (2015). Sensitivity of the initiation of debris flow to initial soil moisture. *Landslides*, *12*(6), 1139-1145. https://doi.org/10.1007/s10346-014-0529-2

Ivanov, V. Y., Bras, R. L., & Vivoni, E. R. (2008). Vegetation-hydrology dynamics in complex terrain of semiarid areas: 1. A mechanistic approach to modeling dynamic feedbacks. *Water Resources Research*, *44*(3). https://doi.org/10.1029/2006wr005588

Kantelhardt, J. W., Koscielny-Bunde, E., Rybski, D., Braun, P., Bunde, A., Havlin, S., 2006. Long-term persistence and multifractality of precipitation and river runoff records. *Journal of Geophysical Research: Atmospheres*, *111*(D1). https://doi.org/10.1029/2005jd005881

Katul, G., Porporato, A., & Oren, R. (2007). Stochastic dynamics of plant-water interactions. *Annu. Rev. Ecol. Evol. Syst.*, *38*(1), 767-791.

https://doi.org/10.5194/egusphere-2025-6014
Preprint. Discussion started: 6 January 2026

https://doi.org/10.1146/annurev.ecolsys.38.091206.095748

Kirchner, J. W. (2009). Catchments as simple dynamical systems: Catchment characterization, rainfall-runoff modeling, and doing hydrology backward. *Water Resources Research*, *45*(2). https://doi.org/10.1029/2008wr006912

Kim, S. (2015). ppcor: an R package for a fast calculation to semi-partial correlation coefficients. *Communications for statistical applications and methods*, *22*(6), 665.

Kursa, M. B., Jankowski, A., & Rudnicki, W. R. (2010). Boruta–a system for feature selection. *Fundamenta informaticae*, *101*(4), 271-285. https://doi.org/10.3233/FI-2010-288

Lazarovitch, N., Vanderborght, J., Jin, Y., Van Genuchten, M. T., 2018. The root zone: Soil physics and beyond. *Vadose zone journal*, *17*(1), 1-6. https://doi.org/10.2136/vzj2018.01.0002

Liu, S., van Meerveld, I., Zhao, Y., Wang, Y., & Kirchner, J. W. (2023). Seasonal dynamics and spatial patterns of soil moisture in a loess catchment. *Hydrology and Earth System Sciences Discussions*, *2023*, 1-26. https://doi.org/10.5194/hess-28-205-2024, 2024

Li, Y. X., Leng, P., Kasim, A. A., & Li, Z. L. (2025). Spatiotemporal variability and dominant driving factors of satellite observed global soil moisture from 2001 to 2020. *Journal of Hydrology*, *654*, 132848. https://doi.org/10.1016/j.jhydrol.2025.132848

Mirus, B. B., Becker, R. E., Baum, R. L., & Smith, J. B. (2018). Integrating real-time subsurface hydrologic monitoring with empirical rainfall thresholds to improve landslide early warning. *Landslides*, *15*(10), 1909-1919. https://doi.org/10.1007/s10346-018-0995-z

Moragoda, N., Kumar, M., & Cohen, S. (2022). Representing the role of soil moisture on erosion resistance in sediment models: Challenges and opportunities. *Earth-Science Reviews*, *229*, 104032. https://doi.org/10.1016/j.earscirev.2022.104032

Neumann, R. B., & Cardon, Z. G. (2012). The magnitude of hydraulic redistribution by plant roots: a review and synthesis of empirical and modeling studies. *New Phytologist*, *194*(2), 337-352. https://doi.org/10.1111/j.1469-8137.2012.04088.x

Nicolai-Shaw, N., Gudmundsson, L., Hirschi, M., & Seneviratne, S. I. (2016). Long-term predictability of soil moisture dynamics at the global scale: Persistence versus large-scale drivers. *Geophysical Research Letters*, *43*(16), 8554-8562. https://doi.org/10.1002/2016GL069847

https://doi.org/10.5194/egusphere-2025-6014
Preprint. Discussion started: 6 January 2026

977 Peng, C., Zeng, J., Chen, K. S., Li, Z., Ma, H., Zhang, X., ... & Bi, H. (2023). Global spatiotemporal
978 trend of satellite-based soil moisture and its influencing factors in the early 21st century.
979 *Remote Sensing of Environment*, *291*, 113569. https://doi.org/10.1016/j.rse.2023.113569
980 Ran, Q., Su, D., Li, P., & He, Z. (2012). Experimental study of the impact of rainfall characteristics
981 on runoff generation and soil erosion. *Journal of hydrology*, *424*, 99-111.
982 https://doi.org/10.1016/j.jhydrol.2011.12.035
983 Salvucci, G. D., & Entekhabi, D. (1994). Equivalent steady soil moisture profile and the time
984 compression approximation in water balance modeling. *Water Resources Research*, *30*(10),
985 2737-2749. https://doi.org/10.1029/94wr00948
986 Schönauer, M., Ågren, A. M., Katzensteiner, K., Hartsch, F., Arp, P., Drollinger, S., & Jaeger, D.
987 (2024). Soil moisture modeling with ERA5-Land retrievals, topographic indices, and in situ
988 measurements and its use for predicting ruts. *Hydrology and Earth System Sciences*, *28*(12),
989 2617-2633. https://doi.org/10.5194/hess-28-2617-2024, 2024
990 Schreiber, T., & Schmitz, A. (2000). Surrogate time series. Physica D: *Nonlinear Phenomena*,
991 *142*(3-4), 346-382. https://doi.org/10.1016/s0167-2789(00)00043-9
992 Song, P., Zhang, Y., Guo, J., Shi, J., Zhao, T., & Tong, B. (2022). A 1-km daily surface soil moisture
993 dataset of enhanced coverage under all-weather conditions over China in 2003–2019. *Earth*
994 *System Science Data Discussions*, *2022*, 1-51. https://doi.org/10.5194/essd-14-2613-2022
995 Van Genuchten, M. T. (1980). A closed-form equation for predicting the hydraulic conductivity of
996 unsaturated soils. *Soil science society of America journal*, *44*(5), 892-898.
997 https://doi.org/10.2136/sssaj1980.03615995004400050002x
998 Valavi, R., Elith, J., Lahoz-Monfort, J. J., & Guillera-Arroita, G. (2018). blockCV: An r package for
999 generating spatially or environmentally separated folds for k-fold cross-validation of species
1000 distribution models. *Biorxiv*, 357798. https://doi.org/10.1101/357798
1001 Varga, C., & Csiszér, L. (2020). The influence of slope aspect on soil moisture. Acta Univ. Sapientiae
1002 Agric. *Environ*, *12*, 82-93. https://doi.org/10.2478/ausae-2020-0007
1003 Wei, L., Song, D., Cui, P., Su, L., Zhou, G. G., Hu, K., ... & Tang, H. (2025). A long-term dataset of
1004 debris-flow and hydrometeorological observations from 1961 to 2024 at Jiangjia Ravine, China.
1005 *Earth System Science Data Discussions*, *2025*, 1-35. https://doi.org/10.5194/essd-2025-190

https://doi.org/10.5194/egusphere-2025-6014
Preprint. Discussion started: 6 January 2026

1006 Western, A. W., Zhou, S. L., Grayson, R. B., McMahon, T. A., Blöschl, G., & Wilson, D. J. (2004).
1007 Spatial correlation of soil moisture in small catchments and its relationship to dominant spatial
1008 hydrological processes. *Journal of Hydrology*, *286*(1-4), 113-134.
1009 https://doi.org/10.1016/j.jhydrol.2003.09.014
1010 Wicki, A., Jansson, P. E., Lehmann, P., Hauck, C., & Stähli, M. (2021). Simulated or measured soil
1011 moisture: which one is adding more value to regional landslide early warning?. *Hydrology and*
1012 *Earth System Sciences*, *25*(8), 4585-4610. https://doi.org/10.5194/hess-25-4585-2021
1013 Wicki, A., Lehmann, P., Hauck, C., Seneviratne, S. I., Waldner, P., & Stähli, M. (2020). Assessing
1014 the potential of soil moisture measurements for regional landslide early warning. *Landslides*,
1015 *17*(8), 1881-1896. https://doi.org/10.1007/s10346-020-01400-y
1016 Xie, P., Joyce, R., Wu, S., Yoo, S.-H., Yarosh, Y., Sun, F., & Lin, R. (2019). NOAA Climate Data
1017 Record (CDR) of CPC Morphing Technique (CMORPH) High Resolution Global Precipitation
1018 Estimates, Version 1 [indicate subset]. NOAA National Centers for Environmental Information.
1019 https://doi.org/10.25921/w9va-q159
1020 Yang, H., Hu, K., Zhang, S., & Liu, S. (2023). Feasibility of satellite-based rainfall and soil moisture
1021 data in determining the triggering conditions of debris flow: The Jiangjia Gully (China) case
1022 study. *Engineering Geology*, *315*, 107041. https://doi.org/10.1016/j.enggeo.2023.107041
1023 Yin, L., Dai, E., Zheng, D., Wang, Y., Ma, L., & Tong, M. (2020). What drives the vegetation
1024 dynamics in the Hengduan Mountain region, southwest China: Climate change or human
1025 activity?. *Ecological Indicators*, *112*, 106013. https://doi.org/10.1016/j.ecolind.2019.106013
1026 Zhang, B., Ouyang, C., Cui, P., Xu, Q., Wang, D., Zhang, F., ... & Zhang, Q. (2024). Deep learning
1027 for cross-region streamflow and flood forecasting at a global scale. *The Innovation*, *5*(3).
1028 https://doi.org/10.1016/j.xinn.2024.100617
1029 Zhang, B., Tian, L., He, C., & He, X. (2023). Response of erosive precipitation to vegetation
1030 restoration and its effect on soil and water conservation over China's Loess Plateau. *Water*
1031 *Resources Research*, *59*(1), e2022WR033382. https://doi.org/10.1029/2022WR033382
1032 Zhang, J., Wu, Z., Li, Y., Qin, C., & Cui, J. (2025). Memory character and predictive period of soil
1033 moisture in the root-zone and along hillslope. *Journal of Hydrology*, 133428.
1034 https://doi.org/10.1016/j.jhydrol.2025.133428

https://doi.org/10.5194/egusphere-2025-6014
Preprint. Discussion started: 6 January 2026

1035 Zhang, J. (2025). Daily Soil Moisture and Its Driving Factors (Static and Dynamic) in Three
1036 Watersheds: Dali River Basin, Anning River Basin, and Jiangjia Ravine (2003-2022) [Data set].
1037 Zenodo. https://doi.org/10.5281/zenodo.17510469
1038 Zhang, J. (2025). Code for: “Scale-Dependent Soil Moisture Memory and Its Driving Mechanisms
1039 in Hazard-Prone Mountain Watersheds”. Zenodo. https://doi.org/10.5281/zenodo.17510622